Geological Magazine

www.cambridge.org/geo

Original Article

Cite this article: Spry PG and Thieben SE. Mineralogy, geochemistry and genesis of alkaline igneous rock-related gold-silver telluride deposits of central Montana. Geological Magazine 162(e41): 1–30. https://doi.org/10.1017/S0016756825100290

Received: 24 April 2025 Revised: 26 August 2025 Accepted: 6 September 2025

Kevwords

Epithermal gold deposits; Gold-silver tellurides; Alkaline igneous rocks; Montana

Corresponding author:

Paul G. Spry; Email: pgspry@iastate.edu

© The Author(s), 2025. Published by Cambridge University Press. This is an Open Access article, distributed under the terms of the Creative Commons Attribution licence (https://creativecommons.org/licenses/by/4.0/), which permits unrestricted re-use, distribution and reproduction, provided the original article is properly cited.



Mineralogy, geochemistry and genesis of alkaline igneous rock-related gold-silver telluride deposits of central Montana

Paul G. Spry¹ and Scott E. Thieben²

¹Department of the Earth, Atmosphere and Climate, Iowa State University, Ames, IA, USA and ²Brushy Creek Minerals, Boone, Iowa, USA

Abstract

Gold-silver telluride deposits in central Montana contain > 400 t Au and are spatially and genetically related to major faults in the Great Falls Tectonic Zone (GFTZ) and the Lewis and Clark Line. They are also related to alkaline igneous intrusive rocks, including monzonites, syenites, diorites, tinguaites, dacites, lamprophyres, and trachytes. Deposit styles include bonanza veins, carbonate replacement at igneous-carbonate contacts, breccia pipe-hosted, and structurally controlled igneous-hosted. Ore-related breccias are a common feature. The ore mineralogy is complex, and locally contains native gold/electrum, Au-Ag tellurides (calaverite, sylvanite, krennerite, petzite, empressite, stützite, and hessite), Bi-tellurides (tetradymite, tellurobismuthite), Bi sulphosalts, and rare precious-metal sulphotellurides. Alteration related to ore-stage fluids is localised primarily adjacent to veins and characterised by silicification, fluoritisation, adularia-sericite, and roscoelite±clays. Fluid inclusion studies suggest that gold telluride ores were deposited from low-temperature (130°-270 °C), moderately saline (1-12 equiv. wt % NaCl), locally boiling, CO₂-poor, near neutral, relatively oxidising fluids. Oxygen and hydrogen isotope studies support the concept that the deposits formed from a continuum between magmatic and meteoric fluids, whereas sulphur isotope compositions of sulphides suggest a magmatic sulphur source or sulphur that was leached from sulphides in volcaniclastic and clastic sedimentary rocks. Lead isotope compositions are permissive of a crustal source with a contribution from Palaeozoic or Proterozoic sedimentary rocks hosting the alkalic igneous rocks. Porphyry molybdenum and Carlin-like Au-Te deposits are also genetically related to the GFTZ and Lewis and Clark Line and represent end-members that form a continuum with epithermal gold-silver telluride deposits.

1. Introduction

Alkaline igneous rock-related gold-silver telluride deposits are among the world's leading sources of gold and include Ladolam, Papua New Guinea (680 t Au; Moyle *et al.* 1990), Emperor, Fiji (255 t Au; G. Begg, unpub. PhD thesis, Monash Univ., 1996), Porgera, Papua New Guinea (340t Au; Richards, 1995), and Cripple Creek deposit, Colorado (595 t Au; Kelley & Luddington, 2002). In the United States, alkaline igneous rock-related gold deposits of Cretaceous-Tertiary age occur in a belt of rocks in the United States Cordillera that extends from Montana to Texas (Mutschler *et al.* 1985). Gold tellurides occur in several of these deposits in the Black Hills, South Dakota (e.g. Paterson *et al.* 1989), the Colorado Mineral Belt (Kelly & Goddard, 1969), Cripple Creek, Colorado (e.g. Thompson *et al.* 1985; Kelley & Luddington, 2002), and the central Montana alkalic province (e.g. Giles, 1983; Childs & Foster, 1993; Foster & Childs, 1993).

Despite the presence of > 400 t Au (produced and reserves) in gold telluride deposits in the central Montana alkalic province (CMAP), evaluations of their geological setting, mineralogy, and geochemistry are restricted to short reviews by Giles (1983), Foster and Childs (1993), Richards (1995), Thieben and Spry (1995), Kelley and Spry (2016), Gammons *et al.* (2020a) and Kelley *et al.* (2020). Giles (1983) discussed the general geological relations between alkalic volcanism and gold mineralisation in the CMAP and identified three main types of gold deposit: 1. Intrusion-hosted disseminated auriferous pyrite; 2. Stockworks and brecciated veins of auriferous quartz-pyrite at intrusive contacts; and 3. Limestone- and dolomite-hosted disseminated replacement deposits adjacent to porphyry contacts. He pointed out the presence of tellurides in several deposits. In describing the geological setting of lode gold systems in Montana, Foster and Childs (1993) gave brief descriptions of several gold deposits, including some that contained tellurides: Beal, Golden Sunlight, York, New World, Gies, Giltedge, Kendall, Spotted Horse, and Zortman-Landusky. They proposed that the deposits were strongly influenced by their structural setting and that they formed as a result of the interaction between structural, magmatic, and sedimentary depositional processes.

Richards (1995) included a brief summary of the CMAP in a worldwide review of alkalic-type epithermal gold deposits. His examination included a discussion of the geological and geochemical setting of the Zortman-Landusky, Gies, and Golden Sunlight deposits. Further reviews of worldwide alkaline igneous rock-related gold deposits by Kelley and Spry (2016) and Kelley *et al.* (2020) also incorporated some deposits in the CMAP.

In addition to the aforementioned regional descriptions of gold telluride deposits in the CMAP, summaries of the geological setting of gold deposits (including gold telluride deposits) in the Judith Mountains were conducted by Weed and Pirsson (1898), R.A. Forrest (unpub. MS thesis, Montana College of Mineral Science and Technology, 1971), Woodward and Giles (1993), and Woodward (1995). Recently, Olinger *et al.* (2024) analysed alkalic igneous rocks in the northern part of the Judith Mountains near these epithermal gold deposits.

The present paper expands on the limited reviews of Richards (1995), Thieben and Spry (1995), Kelley and Spry (2016), and Kelley et al. (2020) by introducing new geological, mineralogical, and geochemical data (major element compositions, fluid inclusions, Pb and S isotopes) for alkaline igneous rock-related Au-Ag±Bi telluride deposits from central Montana. These data complement earlier studies by us on the Gies (Zhang & Spry, 1991; 1994a,b; Spry & Thieben, 1996; Bindi et al. 2006), Mayflower (Spry & Thieben, 1996) and Golden Sunlight Au-Ag telluride deposits (Spry et al. 1999, 1997). The aim of the contribution is to place limits on physicochemical conditions of ore formation and to provide improved exploration guides for alkaline igneous rockrelated gold telluride deposits in Montana and elsewhere. The Golden Sunlight, Mayflower, Zortman-Landusky, and Kendall deposits are evaluated here, along with a group of small goldtelluride deposits (Gies, Maginnis, Spotted Horse, Giltedge, Kentucky Favourite) in the Judith Mountains. Sulphur isotope compositions obtained herein of some non-telluride bearing deposits in the Judith Mountains (American Flag, Black Bull, Butcher Knife, Gold Hill, Great Falls and Judith, Iron Chancellor, Justice, Matthews and Last Chance, Silver Bullion), which occur in close proximity to gold telluride deposits, are included in this study for comparative purposes. Tellurides have been reported in other deposits in Montana (e.g. Beal Au-Bi, New World Au-Cu-Ag, Virginia City Au-Ag, Stillwater Pt-Pd) but are not included here because they are not spatially associated with alkaline igneous rocks in the CMAP (Cabri et al. 1979; Hastings & Harrold, 1988; Johnson & Meinert, 1994; Gammons et al. 2019).

It should be noted here that although alkaline igneous rock-related gold telluride deposits are mainly mined for gold and silver, they are also potential sources of tellurium, which is considered to be a critical element for use in the green energy transition (McNulty & Jowitt, 2022).

2. Regional geology

The regional geology of Montana has been described by Foster and Childs (1993) and Lageson *et al.* (2020) and is summarised here. Early to Late Archaean greenschists and granulites occur in south-central Montana and are overlain by a thick sequence of Middle Proterozoic to Cenozoic carbonate and clastic sedimentary rocks. Igneous rocks range in age from Archaean to Pleistocene. Foster and Childs (1993) informally divided Montana into the Basement, Fold-Thrust and Plains Tectonic Provinces, based on differences in deformation styles. This is a modification of the terminology originally proposed by McMannis (1965), who first identified four

provinces. The Basement Province occurs in southwest Montana, consists of Archaean crystalline basement and Palaeozoic sediments, and is characterised by thick-skinned foreland-style deformation. The Fold-Thrust Province occupies western Montana and consists of Proterozoic and younger sedimentary rocks, exhibiting thin-skinned, thrust belt-style deformation. The Plains Province is composed of Mesozoic and Cenozoic sedimentary rocks and is found in central and eastern Montana, where broad folds and basins were produced along reactivated basement structures.

Pirsson (1905) first identified the alkalic nature and petrologic similarities of multiple intrusive complexes of Cretaceous to Eocene age throughout central Montana and was the first to refer to this region as the 'central Montana alkalic province'. Although Pirsson suggested that the south end of the CMAP was at the southern end of the Big Belt Mountains, Larsen (1940), in recognising alkalic rocks in several mountain ranges in Montana, extended the province from Yellowstone Park to the Canadian border. However, due to the presence of alkaline igneous rocks in association with the Golden Sunlight and Mayflower gold-silver telluride deposits near Whitehall, Montana, the current contribution reinforces the concept of Foster and Childs (1993) that the CMAP extends further to the southwest than that proposed by Larsen (1940).

The orogenic and tectonic evolution of Montana is complex and is described in detail by Lageson et al. (2020). A fundamental northeast-trending structural zone that extends from southwestern Idaho to Saskatchewan is known as the Great Falls Tectonic Zone (GFTZ) in Montana (O'Neill & Lopez, 1985) and the trans-Challis fault system in Idaho (Kiilsgaard & Lewis, 1985). Lageson et al. (2020) described the SW extension of the GFTZ as being the Big Sky Orogen. It should be noted that the GFTZ hosts all known gold-telluride deposits in Montana (Fig. 1), and that it essentially parallels another major gold-telluride-bearing structural zone along the eastern edge of the U.S. Cordillera, the Colorado Mineral Belt. Like the GFTZ, another major tectonic feature in Montana, the NW-SE trending Lewis and Clark Line or Montana Lineament, has been reactivated and mineralised since the Precambrian (Foster & Childs, 1993). Periodic episodes of igneous activity, especially during the Late Cretaceous to Eocene, were localised along these two intersecting zones in the three tectonic provinces identified by Foster and Childs (1993).

The plate tectonic setting of the CMAP and the GFTZ is controversial. O'Neill and Lopez (1985) proposed that the GFTZ may form the contact between Precambrian crustal terranes, whereas Mutschler et al. (1991) suggested that the GFTZ may have been a transtensional zone or a releasing bend between transcurrent faults during the Cretaceous. More recently, Boerner et al. (1998) discounted the idea that the GFTZ is a Proterozoic age suture between the Archaean Hearn and Wyoming provinces but represents a reactivated Archaean intracontinental shear zone. K-Ar and Rb-Sr ages of approximately 1.6 Ga for the GFTZ were reported by, for example, Giletti (1966), but older zircon U-Pb ages of 1.87-1.86 Ga for diorite in the GFTZ suggest that the zone may have been reactivated, with Mueller et al. (2002) identifying Palaeoproterozoic crust within the GFTZ. Regardless of the origin of the GFTZ, the interpretation of magnetic and gravity data by Kleinkopf (1991) led to the conclusion that fractures in the Precambrian basement in the GFTZ influenced the emplacement of the alkalic intrusive complexes. Heat-flow modelling and seismic tomography studies by Eggler and Furlong (1991) suggested that a thick Precambrian lithosphere or mantle keel

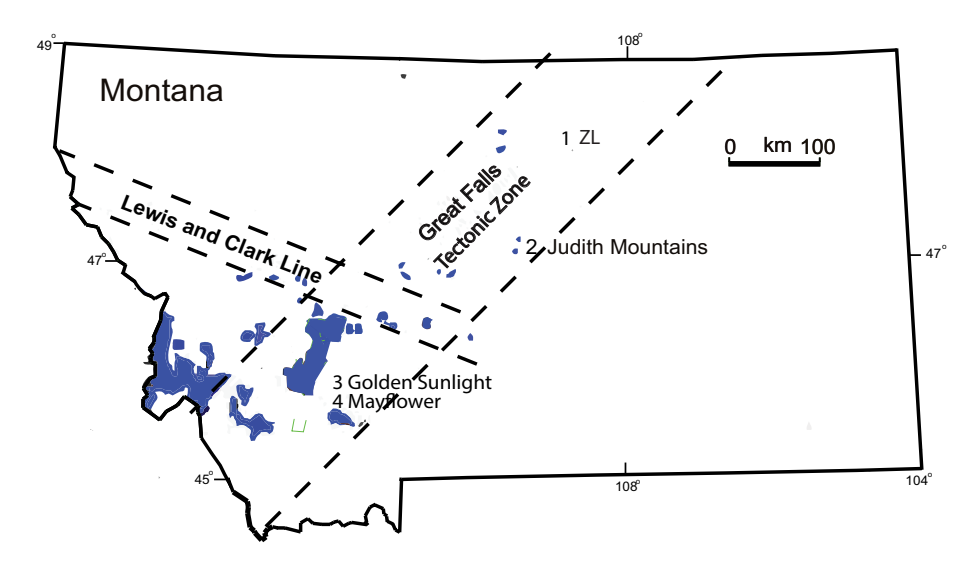


Figure 1. Location of gold telluride deposits in Montana. 1. ZL = Zortman-Landusky; 2. Judith Mountain deposits (Gies, Spotted Horse, Maginnis, Giltedge, Kentucky Favourite); 3. Golden Sunlight district; 4. Mayflower. Late Cretaceous to Tertiary intrusions are shown in blue. Note the location of the deposits relative to the Great Falls Tectonic Zone and the tectonic Lewis and Clark Line is indicated (modified after Vuke *et al.* 2009; Gammons *et al.* 2020b).

underlies central Montana and probably served as an impediment to low-angle SW to NE subduction of the Farallon Plate. Eggler et al. (1988) and Eggler and Furlong (1991) proposed a back-arc advection model for the origin of CMAP in which a steeply dipping subduction zone produces circulation of the asthenosphere and magma generation from a partially melted lithosphere. As was discussed by Baker (1992), the back-arc advection model of Eggler et al. (1988) is in contrast to that proposed by Bird (1998), who invoked a flat-slab subduction model for the Farallon Plate. Lageson et al. (2020), more recently, while invoking the importance of the Farallon Plate, suggested that it decoupled from the North American Plate and was associated with SW rollback and its removal beneath the Rocky Mountain foreland.

3. Analytical methods

Samples in this study were collected from underground localities, drill core, operating pits, and surface dumps and examined using an Olympus dual reflected-transmitted light petrographic microscope, with selected samples being subjected to scanning electron microscope, electron microprobe and ion microprobe studies. Chemical compositions of native elements, tellurides, sulphides, and sulphosalts were obtained using an ARL-SEMQ electron microprobe. The standards used were pure metals (for Au, Ag, Te, Se, and Cu), AgBiS₂ and Bi₂S₃ (Bi), Sb₂S₃ (Sb), As₂S₃ (As), ZnS (Zn), HgS (Hg) and Fe_{0.939}S (Fe and S). Operating conditions included an accelerating voltage of 20 kV and sample currents of 20 nA. The ARL-SEMQ electron microprobe employed the PRSUPR data-reduction procedures (Donovan et al. 1992). Scanning electron microscope studies were conducted on Hitachi S-2460N and JEOL JSM-35 instruments that possessed EDAX area mapping and back-scattered imaging capabilities.

Gold and arsenic contents of pyrite and marcasite were obtained using a Cameca MS-3f ion microprobe at Advanced Mineral Technology Laboratory (AMTEL), London, Ontario, Canada. Experimental parameters and operating conditions are given in Spry and Thieben (2000). The measurements were done with a primary Cs⁺ beam source of about 50-55 nA at 14.5 keV in high-mass resolution mode with –180V offset to eliminate interference with $^{197}\text{FeAsS}_2$. The primary ion beam diameter was 20 μm , and the depth of most analyses was, in general, up to 1.2 μm .

Some ion sputtering to depths of 4 μm was done to evaluate whether gold and, if present, how much gold was distributed throughout the volume of pyrite grains. Calibration of Au and As was done by external standardisation using gold-implanted arsenopyrite (Chryssoulis *et al.* 1989). A minimum detection limit of 150 ppb Au was obtained.

Fluid inclusion studies of quartz in samples from the Spotted Horse deposit were done on a Fluid Inc.-adapted U.S. Geological Survey gas flow heating/freezing stage calibrated with synthetic fluid inclusions at Iowa State University. The estimated accuracy is $\pm~0.1^{\circ}\text{C}$ between -56.6 and 100 °C, and $\pm2^{\circ}\text{C}$ at 374.1 °C. Reproducibility is within the estimated accuracy of the temperature determination.

Major element (SiO₂, Al₂O₃, Fe₂O₃, CaO, MgO, Na₂O, K₂O, MnO, TiO₂, P₂O₅, Cr₂O₃, LOI) compositions of igneous rocks from the Mayflower deposit and deposits in the Judith Mountains were determined by LiBO₂ fusion and measured by ICP-AES techniques. Trace elements (Ba, Nb, Ni, Sc, Sr, Y, Zr) were obtained by LiBO₂ fusion, where the sample was then dissolved in 5% nitric acid, and measured by ICP-MS techniques by Acme Analytical Laboratories. Standards used by Acme Analytical Laboratories are accurate to within $\pm 5~\mu g/g$ for the trace elements and to within $\pm 2~\mu g/g$ percent for major elements. Exceptions are for Ni, Nb and Sc, which are all below the limits of detection (20, 50, and $10~\mu g/g$, respectively).

Samples for sulphur isotope analysis were either hand-picked or drilled with a Dremel tool and inspected under a binocular microscope to insure a purity of >95%. Sulphur isotope compositions were obtained from the Departments of Geology at Indiana University and the University of Georgia. At these locations, sulphide separates were converted to SO_2 by combustion with V_2O_5 , utilising the methods described by Yanagisawa and Sakai (1983). Analyses were run on Finnigan Mat 252 mass spectrometers. The isotopic ratios are reported in the standard δ notation in per mil relative to Cañon Diablo troilite (VCDT). The precision of analysis was ± 0.15 per mil at Indiana and ± 0.20 per mil at Georgia based on replicate analysis of standards.

Lead isotope compositions of galena were measured at the University of Washington using the procedure of McCallum *et al.* (1999). The process involves a progressive acid leaching procedure to remove any contamination on grain boundaries and fracture

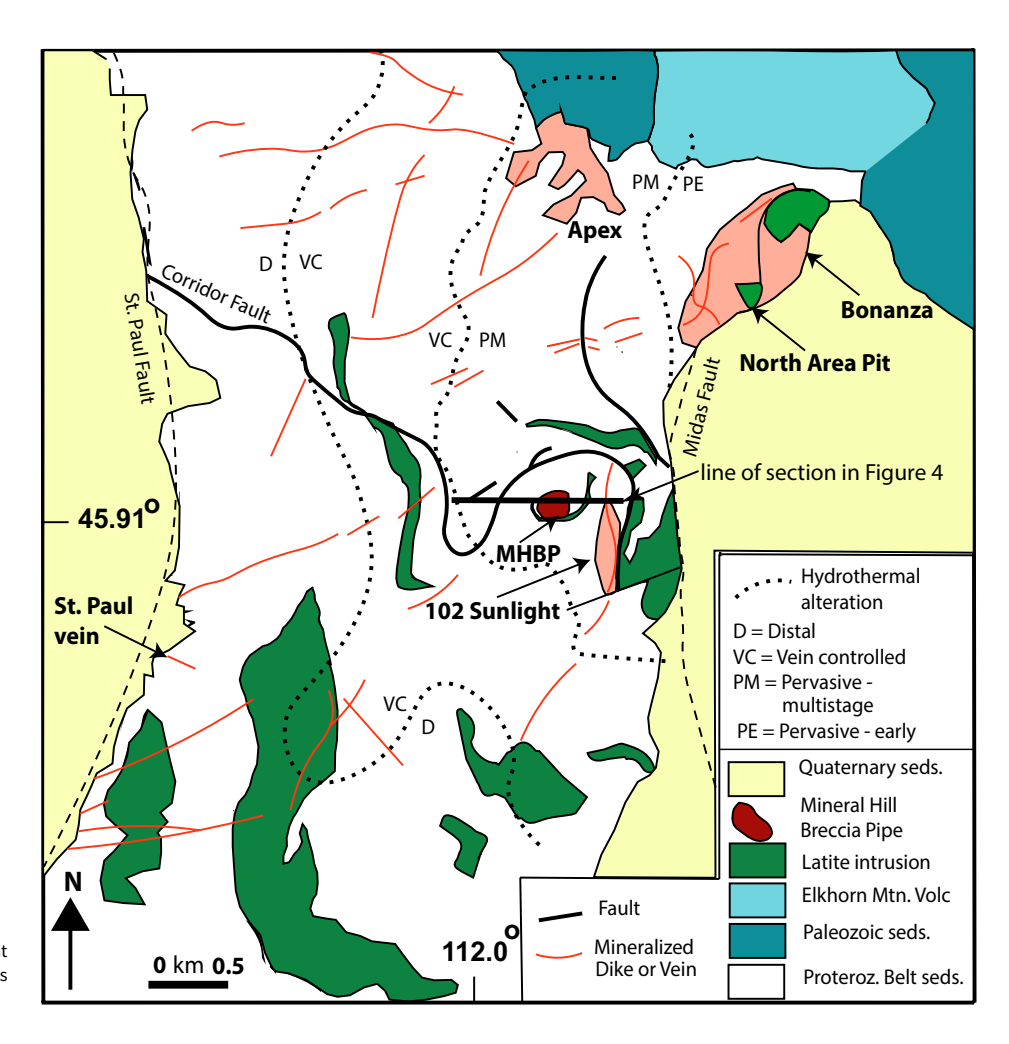


Figure 2. Geological map of the Golden Sunlight district (modified from Spry *et al.* 1996; Gammons *et al.* 2020b).

surfaces and to preferentially leach unsupported radiogenic Pb. Between two and six leaches were extracted from each sample, depending on sample size. Aliquots of each leach were prepared for isotopic composition and isotopic dilution measurements. Fifty to 100 ml of anion exchange resin (AG1X8 200 ± 400 mesh) was used for separation and purification of Pb. The isotopic measurements were obtained on a VG-Sector mass spectrometer. Isotopic measurements were made between 1150 and 1350 °C using static multicollection. Scans between masses 200 and 210 were made to check for interference peaks from organic compounds or BaPO₂, ²⁰³Tl, and ²⁰⁵Tl. Multiple measurements of a standard (NBS-981) showed mass fractionation of 0.125% per amu (atomic mass unit). All analyses were corrected for mass fractionation and blank contribution. The internal precision of the isotopic measurements is less than <0.1% based on multiple analyses of NBS981 and an internal lab sulphide standard (4750E-ST).

4. Geological setting of Au-Ag telluride deposits

4.a. Golden Sunlight district, Whitehall

The epithermal Golden Sunlight Au-Ag-Te-Bi-Mo deposit is genetically associated with a Late Cretaceous alkaline to subalkaline porphyry system. The mining operation was in continuous

operation between 1982 and 2022, and produced more than 102 t Au, with an average ore grade of ~ 1.5 g/t Au. Previous studies of the Golden Sunlight deposit consist of those by AE Lindquist (unpub MS thesis, Montana Technical University, 1966), who described its general geological setting and by Porter and Ripley (1985), Spry et al. (1996) and Spry and Thieben (1999), who evaluated the mineralogical, stable isotope and fluid inclusion characteristics of the ore deposit. DeWitt et al. (1996) determined the chronology of igneous and hydrothermal events in the Golden Sunlight mine area, while Spry et al. (1997) and Spry and Thieben (2000) completed mineralogical investigations of the ore. Recent studies by Gammons et al. (2020b) extended these earlier studies by focusing on sulphide mineralisation in locations (Apex, Bonanza, 102 Sunlight, and North Area Pit) peripheral to, but within 2 km of the main Golden Sunlight deposit (Fig. 2), while Zhao et al. (2025) provided sulphur and He-Ar isotopic constraints on the origin of the deposit.

The local geology is described in detail by Foster and Childs (1993), Childs and Foster, (1993), DeWitt *et al.* (1996), Spry *et al.* (1997) and Oyer *et al.* (2014) and is briefly summarised here (see also Table 1). Mesoproterozoic sedimentary rocks that host the Golden Sunlight deposit can be divided into two units; the older LaHood Formation, consisting of arkoses, sandstones, conglomerates, and carbonaceous black shales, and the informally named

Table 1. Characteristics of selected alkaline igneous rock-related gold telluride deposits, Montana

District, deposit	Zortman-Landusky	Judith Mountains (Spotted Horse, Gies, Cumberland)	Moccasin Mountains (Kendall, Muleshoe deposits)	Golden Sunlight	Mayflower
Deposit type(s)/style	Intrusion-hosted	Vein, contact, carbonate-hosted	Contact, carbonate- hosted, vein, breccia- hosted	Porphyry Mo, epithermal, breccia- hosted	Vein, replacement
Gold content (grade and tonnage)	109 Mt @ 0.55 g/t, 59.4 t Au	Gies: 1191 kg Au @ 13.7 g/t Au. Spotted Horse: 4969 kg Au @ ~80 g/t Au	4 Mt @ 1.7 g/t, 20.8 t Au	68 Mt @ 1.5 g/t, 102 t Au	W. Mayflower - 121,564 t @ 32.97 g/t Au and 205.9 g/t Ag, Mayflower - 12,700 t @ 85.84 g/t Au, 488.9 g/t Ag
Age (Ma)	67–60	69-59 and 47.8	66–65	82-77	79–78
Alkalic rocks	Stocks and laccoliths of syenite porphyry, breccia pipes and breccia dykes were emplaced in altered syenite porphyry	Stocks, laccoliths, sills, and dykes of Qtz diorite, monzonite, syenite, alkali syenite, and tinguaite; some breccia pipes intrude alkaline igneous rocks	Laccolith complex (including sills and dykes) of alkali syenite, Qtz monzonite, and syenite porphyry; development of breccia pipes within syenite porphyry	Dykes, sills, and stock- like bodies of Qtz monzodiorite, latite porphyry, and lamprophyres	Syenite sill, trachyte and trachyandesite flows of the Elkhorn Mountains Volcanics
Mineralisation style/ structural setting	Vein and disseminated mineralisation in syenite; higher grade zones are localised in regional shears, Ore bodies formed as a result of repeated fault movement or reopening along intrusive contact	Mineralised breccia at contact between limestone and monzonite porphyry, and within limestone and porphyry. Fissure fillings, stockwork veins, breccia cement and replacement styles are common. Minor associated skarns. Four stages recognised (Gies deposit); stage 3 is the telluride stage	Disseminated and stockwork veins; replacement in carbonate sedimentary rocks along contact with intrusive syenite, ore bodies formed as a result of repeated fault movement or reopening along intrusive contact	In chronological order: Proterozoic stratabound sulphides, low-grade porphyry Mo, and epithermal Au in Mineral Hill breccia pipe. Au occurs in disseminations and structurally controlled veins in four stages	Precious metal mineralisation occurs in veins, dolomite, silicified limestone, shale, breccias, and replacement bodies. Five stages recognised with native gold and tellurides in stages 3, 4 (bonanza grades), and 5. Sulphotellurides also in stage 4.
Metallic minerals	Py, Mrc, Apy, Gn, Sp, Aca, Ccp, Au, Clv, Knn, Syv, Hes, Ptz, Eps, Stz, Alt, Clr, Mlt, Te, Tbi, Wst, Rkd, Cvl (?), Smy, Jal, Ag, Plb,	Gies: Py, Sp, Gb, Bn, Ccp, Mc, Col, Ttr, Tnt, Syv, Knn, Hes, Stz, Ngy, Bln, Imi; Spotted Horse: Syv, Ptz, Au, Py, Sp, Gn, Ccp Cumberland: Au, Syv	Au, Au-Te tellurides, sp, gn, py	Golden Sunlight district: Py, Ccp, Sp, Gn, Bn, Mol, Tnt, Ttr, Elc, Au, Pea, Aik, Ttd, Gf, Clv, Ptz, Bhr, Knn, Clr, Stn, Wtc, Ida	Py, Mrc, Fb, Ttr, Syv, Ptz, Hes, Stz, Clv, Au, Alt, Bln, Ngy, Cvl, Te, Ccp, Sp, Gn, Cc, Aca (?)
Trace element association	Au, Ag, Te, As, F	Au, Ag, Te, V, F (latter two in roscoelite and fluorite) which are associated with higher grades of ore.	Au, Ag, Te, V, F	Dominantly Au, Ag, Te, Cu, Bi, and Mo	Dominantly Cu, Pb, Au, Ag, Te, V
References	Lindsey and Fisher (1985), Hastings (1988), Wilson and Kyser (1988), Ryzak (1990), Russell (1991)	Weed and Pirsson (1898), Woodward and Giles (1993), Zhang and Spry (1991, 1994b), Woodward (1995), Spry and Thieben (1996)	Lindsey (1985), Lindsey and Naeser (1985), P. Racenet (unpub. MS thesis, Univ. Montana, 1994)	Porter and Ripley (1985), DeWitt <i>et al.</i> (1996), Spry <i>et al.</i> (1996, 1997); Spry and Thieben (2000), Gammons <i>et al.</i> (2022b)	Cocker (1993), Spry and Thieben (1996)

Mineral abbreviations: Aca acanthite, Ag native silver, Aik aikinite, Alt altaite, Apy arsenopyrite, Au native gold, Bhr buckhornite, Bln benleonardite, Bn bornite, Cc chalcocite, Ccp chalcopyrite, Clr coloradoite, Clv calaverite, Col colusite, Cth clausthalite, Cvl cervelleite, Dig digenite, Elc electrum, Emp emplectite, Eng enargite, Eps empressite, Fb freibergite, Gf goldfieldite, Gn galena, Hem haematite, Hes hessite, Ida idaite, Imi imiterite, Jal jalpaite, Knn krennerite, Ln lenaite, Mag magnetite, Mlt melonite, Mol molybdenite, Mrc marcasite, Mtd matildite, Ngy nagyagite, Pea pearceite, Plb polybasite, Ptz petzite, Py pyrite, Pyh pyrrhotite, Rkd rickardite, Sbn stibnite, Smy stromeyerite, Sp sphalerite, Stn stannite, Stz stützite, Syv sylvanite, Tbi tellurobismuthite, Te native tellurium, Tnt tennantite, Ttd tetradymite, Ttr tetrahedrite, Wst weissite, Wtc wittichenite. Format modified after Jensen and Barton (2000) and Kelley and Spry (2016); mineral abbreviations after Warr (2021).

Bull Mountain Group, which is composed of siltstones, shales, synsedimentary sulphide (primarily pyrite), carbonate and silicate concretions, and olistostromes.

A Cretaceous alkalic-subalkalic suite of igneous rocks consisting of dykes, sills and stock-like bodies of quartz-monzodiorite, latite to rhyolite porphyry, and lamprophyres intrude the Proterozoic rocks. The composition of igneous rocks

associated with the Golden Sunlight deposit, and other telluridebearing gold deposits in Montana, is shown in Figure 3. Latite porphyry is coeval approximately with formation of the Mineral Hill breccia pipe since the porphyry is locally cross-cut by the Mineral Hill breccia pipe, clasts of latite porphyry occur in the breccia, and large bodies of latite porphyry occur at the bottom of the breccia pipe (Fig. 4). A whole-rock model 3 isochron age of

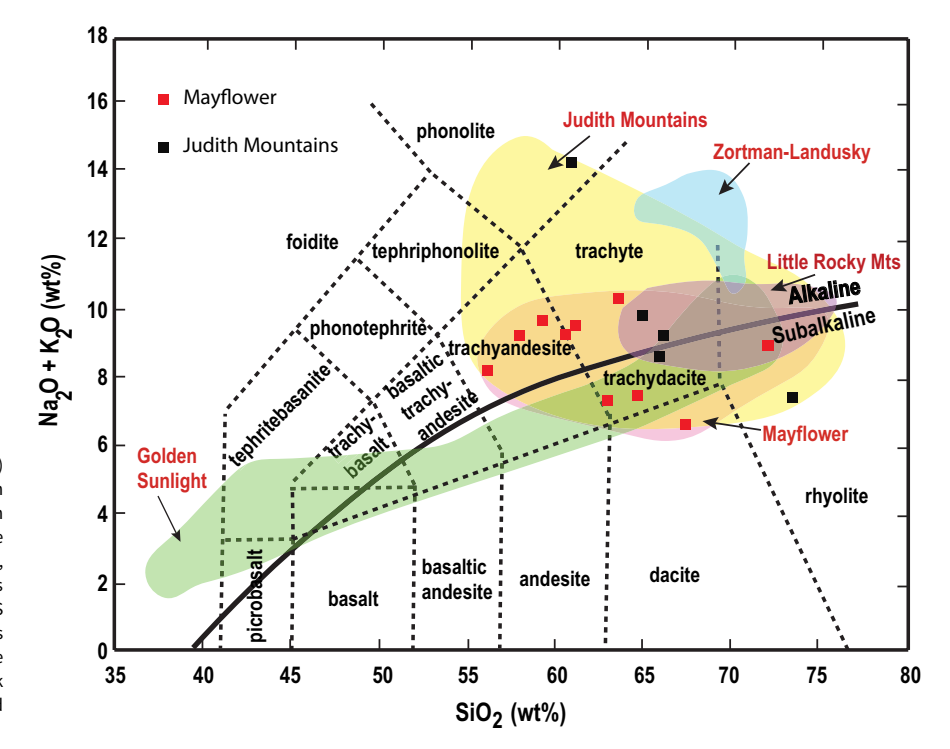


Figure 3. Total alkali vs silica diagram (Le Bas *et al.* 1986) of igneous rock compositions spatially associated with alkaline rock-related epithermal gold-silver deposits in Montana. The alkali-subalkalic boundary is from Irvine and Baragar (1971). Data are from: Mayflower (this study), Golden Sunlight (DeWitt *et al.* 1996), Judith Mountains (Wallace, 1953; Nockolds, 1954; GL Kirchner, unpub MS thesis Univ of Montana 1982; Zhang & Spry, 1994b; this study), Zortman-Landusky (Wilson & Kyser, 1988), Little Rocky Mountains (Russell, 1991). The new whole-rock compositions obtained here for the Mayflower deposit and the Judith Mountains are indicated.

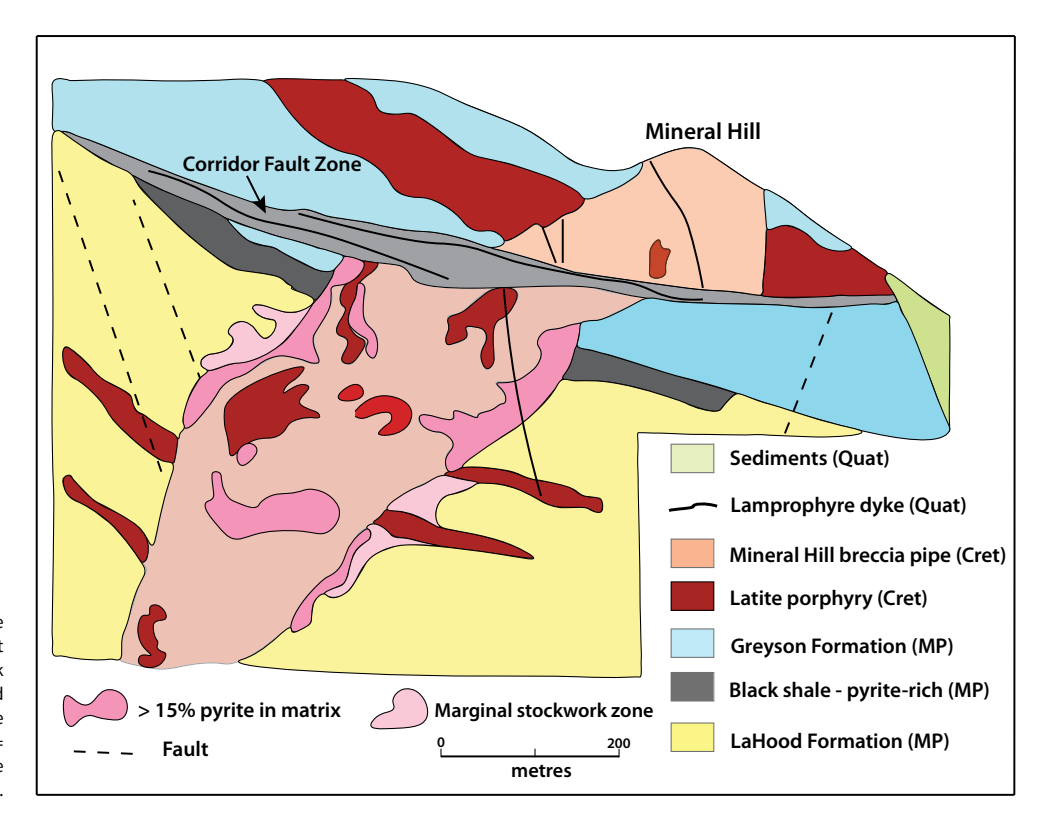


Figure 4. Geological cross-section of the Mineral Hill breccia pipe, Golden Sunlight deposit, showing the location of stockwork zones on the margin of the breccia pipe and zones of hydrothermal alteration where the pyrite content is >15%. Abbreviations: Quat = Quaternary; Cret = Cretaceous; MP = Middle Proterozoic (modified after DeWitt *et al.* 1996).

 84 ± 18 Ma was derived by De Witt *et al.* (1996) while biotite separates from basalts lamprophyres yielded a K-Ar age of 79.8 \pm 2.8 Ma and a 40 Ar- 39 Ar plateau date of 76.9 \pm 0.5 Ma

(DeWitt *et al.* 1996). These ages are comparable to recent 40 Ar- 39 Ar dates of 78.6 \pm 1.5 to 77.5 \pm 1.1 Ma for biotite from latite porphyry at the Bonanza prospect (Gammons *et al.* 2020b).

Ignoring the imprecise whole-rock U-Pb date of DeWitt *et al.* (1996), Gammons *et al.* (2020b) suggested that the age of mineralisation in the district occurred at 81.8 to 76.9 Ma.

The Mineral Hill breccia pipe, which plunges at an average angle of 35° to the southwest (Fig. 4), has a circular to elliptical plan with a diameter of up to 270 m and a vertical extent of >700 m, and consists of fragments of Proterozoic sedimentary rocks and latite that range in size from a few millimetres to >10 m in diameter. Relatively unaltered potassic trachybasalts, basaltic andesites, and lamprophyre crop out approximately 1.5 km south of the breccia pipe (DeWitt *et al.* 1996), and an altered body of quartz monzodiorite is located 1 km northeast of the pipe. A high concentration of lamprophyre sills is present in the breccia pipe coincident with a deformation zone (Fig. 2).

4.a.1. Hydrothermal mineralisation of the Mineral Hill breccia pipe

Three main types of sulphide mineralisation are found in the district. In chronological order, they are listed as follows: Proterozoic stratabound sulphide mineralisation; the low-grade Mineral Hill porphyry Mo system; and the Mineral Hill breccia pipe and related auriferous veins. Spry et al. (1997) considered the Proterozoic stratabound sulphide mineralisation to be syngenetic or diagenetic in origin. Fluid inclusion, stable isotope and mineral alteration studies by Spry et al. (1996) suggested that the Mineral Hill breccia pipe and related auriferous veins were spatially and temporally linked to the porphyry molybdenum system. This system, which covers a surface area of 6 km², is centred on the Mineral Hill breccia pipe. The general characteristics of the three ore types are described in detail by Spry et al. (1996, 1997), and only the gold mineralisation is discussed here. Details of the mineralogy of the Apex, Bonanza, North Pit and 102/Sun zones are given in Gammons et al. (2020b), where they contain most of the same minerals present in the Mineral Hill breccia pipe, along with goldfieldite, celestite, albite, svanbergite, panasqueraite, and althausite in some of the zones.

Gold mineralisation in the Mineral Hill breccia pipe occurs primarily as disseminations and as structurally controlled northeast- and east-northeast-trending veins and breccias along faults and joints primarily. Most of the gold occurs at the margins of the Mineral Hill breccia pipe. Disseminated mineralisation is located in the sulphide-rich matrix of the breccia, the latite porphyry, and in Proterozoic sedimentary rocks. The highest gold grades (up to 740 g/t) occur in the deepest parts of the breccia pipe.

A new four-stage paragenetic sequence of hydrothermal mineralisation in the breccia pipe, in addition to the porphyry Mo stage, is given in Supplementary Figure S1, which incorporates the mineralogical studies of Porter and Ripley (1985), Spry et al. (1997), Spry and Thieben (2000), Gammons et al. (2020b) and Gammons and Singh (2024). Stages I and IV comprise about 99% of the total volume of the quartz-bearing breccia pipe matrix. Pyrite is the most common sulphide and constitutes up to 20% of some rocks. Stage I consists of two sub-stages, Ia and Ib, whereby haematite, rutile, pyrrhotite, and rare tetradymite occur as inclusions (stage Ia), up to 30µm in length, in the cores of pyrite porphyroblasts. Stage Ib mineralisation is composed of sulphides and sulphosalts that occur as randomly distributed inclusions in stage I pyrite and baryte. Spry et al. (1997) and Spry and Thieben (2000) showed that these inclusions consist of native gold, calaverite, tetradymite, tellurobismuthite, buckhornite, melonite, coloradoite, altaite, clausthalite, stannite, bornite, chalcopyrite, chalcocite, tennantite, sphalerite, wittichenite, emplectite, idaite,

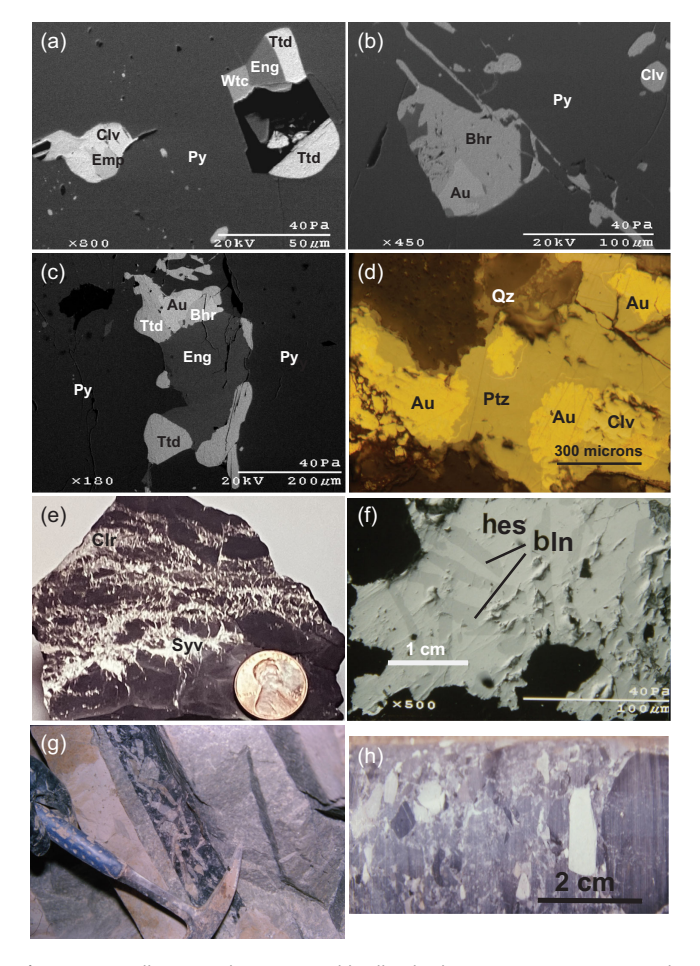


Figure 5. Metallic mineralisation in gold telluride deposits in Montana. a. Back-scattered electron image of inclusions of calaverite (Clv), wittichenite (Wtc), emplectite (Emp), and tetradymite (Ttd) in pyrite (Py) from the Mineral Hill breccia pipe, Golden Sunlight deposit. b. Back-scattered electron (BSE) image of inclusions of buckhornite (Bhr) intergrown with native gold (Au) and calaverite in pyrite from the Mineral Hill breccia pipe, Golden Sunlight deposit. c. BSE image of an intergrowth of native gold, buckhornite, tetradymite and enargite (Eng) in pyrite from the Mineral Hill breccia pipe, Golden Sunlight deposit. d. Plane-polarised reflected light image of intergrown petzite (Ptz), native gold, and calaverite in quartz, Mayflower deposit. e. Sample of high-grade sylvanite (Syv) and coloradoite (Clr) ore in shaley limestone, Mayflower deposit. f. BSE image of benleonardite (Bln) blades in hessite (Hes), Mayflower deposit. g. Gold-bearing brecciated ore in Gold Hill quartz monzonite porphyry, Spotted Horse deposit. h. Polylithic gold-bearing breccia consisting of angular and rounded clasts of monzonite and limestone with calcite in the matrix, Kentucky Favourite deposit.

and petzite and native tellurium (Fig. 5a-c). A recent study by Gammons and Singh (2024) also pointed out the presence of previously unreported hodrusite, mawsonite and goldfieldite in samples containing pyrite and calaverite, which suggests they formed in stage 1b.

Stage II is separated from stage I by a period of brecciation (Porter & Ripley, 1985). Chalcopyrite is the most common mineral in stage II, although pyrite, galena, tennantite, marcasite, and tellurobismuthite, sylvanite, hessite, gold, altaite, and native tellurium are also present. Stage III mineralisation is of relatively minor importance but consists of tennantite that replaced chalcopyrite, and the following precious metal tellurides: petzite, sylvanite, krennerite, hessite, and rare grains of gold and empressite. Stage IV is characterised by infillings between breccia fragments and veins of quartz, pyrite, magnesite, dolomite, kaolinite, fluorapatite, fluorite, dickite, sericite, and chalcopyrite.

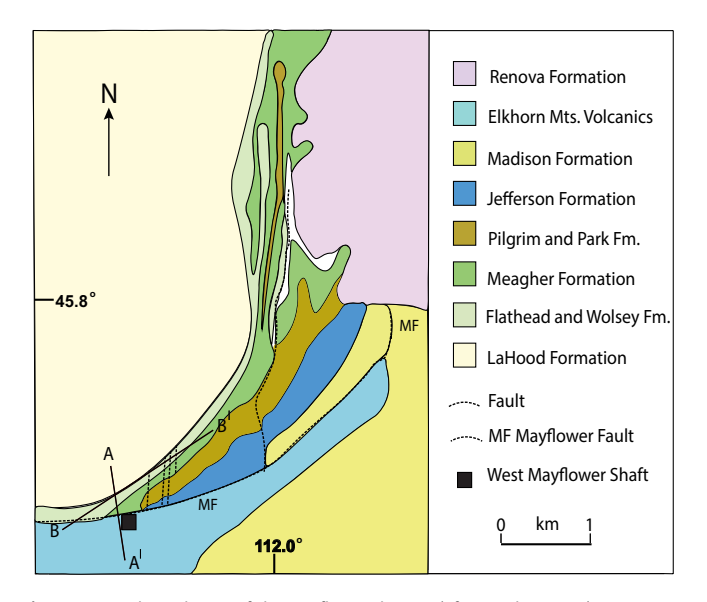


Figure 6. Geological map of the Mayflower deposit (after Cocker, 1993).

4.b. Mayflower deposit, Whitehall

The Mayflower deposit is an epithermal gold vein deposit hosted in dolomite and dolomitic limestone of the Cambrian Meagher Formation. It is spatially related to Late Cretaceous intrusive andesite sills and extrusive Elkhorn Mountains Volcanics (EMV). The deposit was intermittently mined from 1896 to 1961 and produced 5,098 kg Au and 31,237 kg Ag (Cocker, 1993). Drilling by Brimstone Gold Corporation in 1997 and 1998 identified total proven and probable reserves of 595 kg Au and 3912 kg Ag, but the deposit remains open at depth. Previous published studies of the Mayflower deposit are limited to those of Cocker (1993) who described the geological setting, primary element dispersion patterns, and hydrothermal alteration associated with the ore, and Spry and Thieben (1996) who described the presence of rare tellurium-bearing minerals, benleonardite (Ag₈(Sb,As)Te₂S₃) and cervelleite (Ag₄TeS) in high-grade samples of ore.

The Mayflower deposit occurs immediately adjacent to the Mayflower Fault and parallels the Proterozoic Willow Creek fault system (Fig. 6). Lochman-Balk (1971) and Cocker (1993) showed that Middle Proterozoic clastic sedimentary rocks of the LaHood Formation are unconformably overlain by a transgressive sequence of lower Palaeozoic sedimentary rocks in the Mayflower mine area (Figs. 6 and 7). Clastic rocks of the Cambrian Flathead Formation occur at the base of the Palaeozoic sequence and are overlain by the Cambrian Wolsey Shale. The Cambrian Meagher Formation consists of three carbonate members (Cocker, 1993): 1. the basal member is a thick-bedded, dark grey limestone; 2. the middle member is a thin-bedded blue-grey and brown limestone, with locally abundant argillaceous units; and 3. the upper member is a light grey limestone. Gold mineralisation is limited to the Meagher Formation, particularly the middle member.

Intrusive rocks in the mine area are restricted to two sills. One of these sills, up to 10 m wide, is hosted by the Wolsey Formation and occurs along strike from the Mayflower deposit. In the mine area, it was propyllitically altered by chlorite, epidote, and calcite (Cocker, 1993). A second sill, up to 9 m wide, was identified by M.D. Cocker (unpub. report to Anaconda Minerals Company, 1983) in drill core and underground. The two sills have bulk compositions and textural characteristics of a syenite and an aplite (Table 2). The age

of these sills is unknown, but it is likely that they are the intrusive equivalents of the extrusive EMV, which formed at ~ 78 Ma (Tilling *et al.* 1968; Schmidt *et al.* 1988). The EMV are well exposed on the south side of the Mayflower Fault and consist of trachyandesite flows, andesitic tuff breccias, rhyodacite welded tuffs, as well as welded and non-welded pyroclastics (Lund & Aleinikoff, 2022).

The presence of silicification and adularia in and adjacent to gold mineralisation and the spatially associated Mayflower Fault suggests a genetic relationship between mineralisation and the fault. The age of the mineralisation is unknown due to a lack of geochronological studies; however, it is likely to have formed during the late Cretaceous to Palaeogene.

4.b.1. Hydrothermal mineralisation and alteration

Samples used in the present study were obtained either from drill core obtained by Brimstone Gold Corporation, dump material, a collection housed in the Mineral Museum at Montana Tech, or from the collection of Mark D. Cocker that was used in his studies (Cocker, 1993). It should be pointed out that nearly all of the goldrich samples, although poorly located, were derived from the Mayflower ore shoot.

The Mayflower ore zone is steeply dipping to vertical in a structure with a strike length of 900 m and a width of 15 to 20 m and in the Cambrian Meagher Formation. The ore occurs in two lens-shaped ore shoots (Mayflower and West Mayflower), which are open at depths. The Mayflower and West Mayflower ore shoots have strike lengths of 15 to 35 m and 70 to 100 m, respectively, and widths of 1 to 5 m and 2 to 7 m, respectively (Figs. 7 and 8). Minor displacement on reverse and strike-slip faults results in the ore shoots being discontinuous.

Gold mineralisation occurs in quartz veins, dolomite, silicified limestone, shale, quartz-rich breccias and shaley limestone as disseminations, vein fillings, and replacement bodies (Cocker, 1993). According to Cocker (1993), alteration consists of silicified cores that grade into potassic zones characterised by adularia, V-muscovite, roscoelite, quartz, pyrite, and rutile. The potassic zone, in turn, grades into a hydrothermal dolomite zone, which may be up to 40 m wide.

Detailed petrographic studies herein suggest a five-stage paragenetic sequence (Supplementary Figure S2). The first two stages in the ore shoots are characterised by pyrite and sphalerite. Stage 1 pyrite and sphalerite are variable in size (up to 0.2 mm in diameter) and show a variety of anhedral grain shapes. Colloform pyrite, in places, is in-filled with sphalerite. Stage 2 sphalerite and pyrite are coarser grained (up to 0.3 mm in diameter) and occur in quartz-dolomite veins that cross-cut stage 1 pyrite-sphaleritedolomite-quartz intergrowths. Stage 3 mineralisation is sulphurpoor and tellurium-rich compared to stages 1 and 2 and occurs as a replacement of stage 2 veins. It consists of native gold, native tellurium, calaverite (AuTe₂), krennerite ((Au,Ag)Te₂), petzite (Ag₃AuTe₂), altaite (PbTe), tetrahedrite, and minor pyrite (Fig. 5d). Stage 4 mineralisation is volumetrically and economically more important and more silver- and base metal- rich than stage 3 mineralisation and occurs as fine to coarse veins of tellurides that, in places, cross-cut stage 3 veins. The bonanza-grade samples reported by Cocker (1993) and Spry and Thieben (1996) are from stage 4 mineralisation (Figs. 5e), which contains electrum, sylvanite ((AuAg)Te₂), stützite (Ag_{5-x}Te₃), petzite, hessite (Ag₂Te), coloradoite (HgTe), altaite, nagyagite (Pb₅Au(Sb,Bi) Te₂S₆), benleonardite, cervelleite, tetrahedrite, tennantite, pyrite, galena, sphalerite, and marcasite, as well as trace chalcopyrite

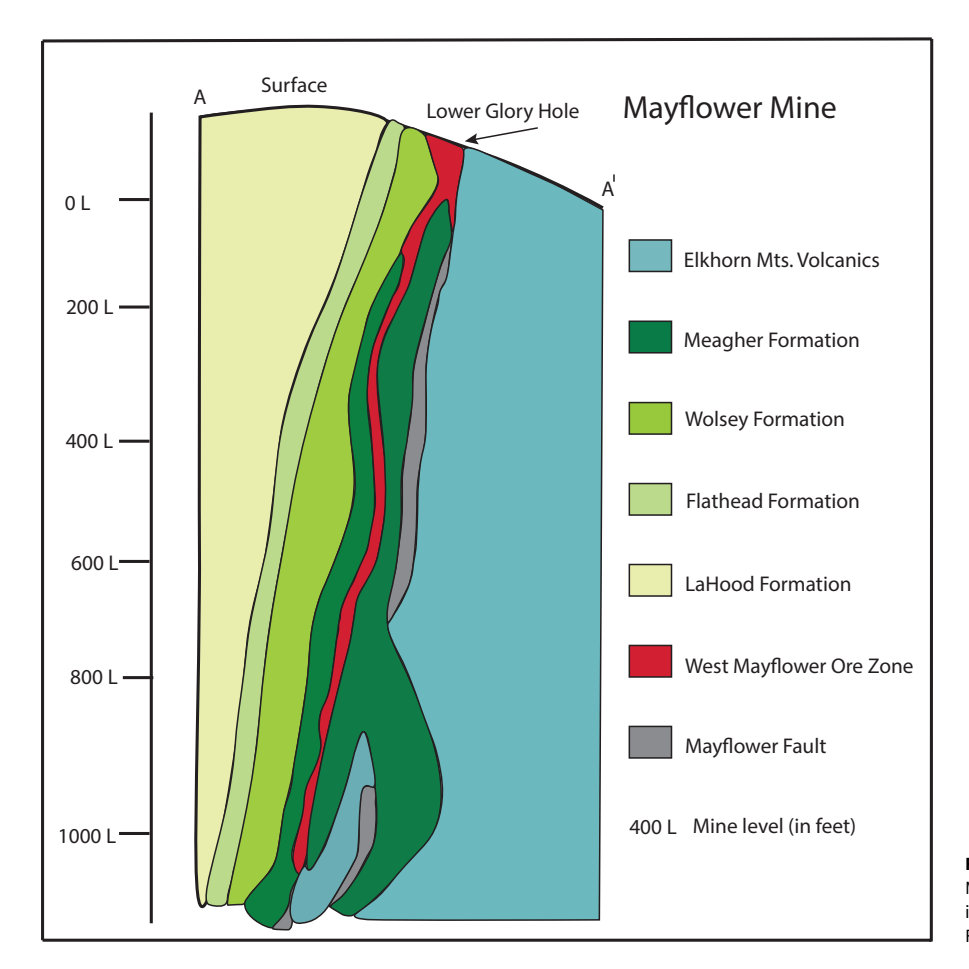


Figure 7. Geological cross-section through the West Mayflower ore zone (after Cocker, 1993). The levels indicated are given in feet. MF refers to the Mayflower Fault

(Fig 5e, f). A variant of stage 4 that occurs in places is a coarse intergrowth of sphalerite, galena, and pyrite that contains trace amounts of hessite, tetrahedrite and chalcopyrite. Rare crosscutting relationships between base metal-rich and base-metal-poor stage 4 veins suggest that the base metal-rich variant of stage 4 may have formed slightly after the base metal-poor variant. By comparison to all other stages, stage 4 mineralisation is also characterised by the greatest variety of gangue and alteration minerals, which include quartz, dolomite, calcite, sericite, roscoelite, chlorite, adularia, zircon and rutile. Stage 5 is rare but consists of an assemblage dominated by Au-rich electrum intergrown with hessite, sphalerite, tetrahedrite, chalcopyrite, sericite, calcite, and quartz, which occur as rims on stage 4 Au-poor electrum.

Native gold/electrum formed in stages 3, 4, and 5 and exhibits a wide range of compositions (Table 3). In stage 3, grains of gold (up to 0.3 mm in diameter) with a fineness of 846-871, are intergrown with calaverite and petzite (Fig. 5d) or occur as isolated grains in quartz or dolomite. A rare assemblage of native gold-petzite-hessite-nagyagite-altaite-pyrite was also observed. Native gold/electrum, with a fineness of 447-820, formed during stage 4 as grains up to 2 mm in length. It occurs in a variety of telluride-bearing assemblages, including electrum-hessite, electrum-hessite-petzite ±galena±sphalerite±pyrite±tetrahedrite, electrum-hessite-benleonardite±tetrahedrite±pyrite± chalcopyrite, electrum-hessite-coloradoite-altaite-galena, as rare intergrowths of native gold-sylvanite-pet zite-stützite-nagyagite-altaite and native gold-petzite-stützite-hessite-galena-pyrite. Overgrowths of electrum, up to 80 µm in width,

with a fineness of 654 to 712 on electrum with a lower fineness, characterise stage 5 assemblages. Inclusions of chalcopyrite, hessite, tetrahedrite, pyrite, quartz, dolomite, calcite, and sericite occur in stage 5 electrum.

Although native gold and electrum are important carriers of gold and silver, precious metal tellurides are more significant. Stage 3 tellurides are generally more gold-rich than stage 4 tellurides since calaverite and krennerite are restricted to stage 3. Calaverite and krennerite occur as intergrowths with native tellurium, whereas petzite and hessite are rare in stage 3. A shift to more silver-rich tellurides in stage 3 is reflected by the presence of sylvanite, petzite, hessite, and stützite, and the absence of calaverite and krennerite. Spectacular samples of coarse stage 4 sylvanite, up to several cm in length, coexisting with native tellurium and with stützite, hessite, petzite, and coloradoite (Figs. 5e) were identified. Representative compositions of tellurides and native minerals are given in Table 3.

A key mineral that distinguishes stage 3 assemblages from stage 4 assemblages is galena. The only Pb minerals in stage 3 are altaite and nagyagite, whereas these minerals and abundant galena characterise stage 4 assemblages. Altaite commonly coexists with hessite and sylvanite in stage 4 veins. Galena is most abundant at the end of stage 4, where it occurs as coarse intergrowths with Fepoor sphalerite (Table 4), pyrite and marcasite. Galena is devoid of trace amounts of Bi, Ag, and Se, and, in this respect, differs considerably from that in the nearby Golden Sunlight gold-silver telluride deposit (5 km from north of Mayflower), which contains galena with up to 6.7 wt % Bi, 6.4 wt % Se, and 4.0 wt % Ag (Spry

Table 2. Whole rock compositions of igneous rocks associated with the Mayflower deposit and Judith Mountains deposits

Sample	1	2	3	4	5	6	7	8
SiO ₂	73.12	64.55	62.74	67.49	56.78	57.23	63.01	61.26
TiO ₂	0.21	0.53	0.71	0.72	0.87	0.88	0.29	0.4
Al ₂ O ₃	12.44	14.02	15.82	13.58	18.19	16.91	15.93	15.95
Fe ₂ O ₃	2.12	5.02	6.28	6.3	7.28	7.33	3.03	3.77
Cr ₂ O ₃	0.02	0.02	0.02	0.02	0.01	0.02	0.02	0.02
MnO	0.01	0.06	0.09	0.06	0.12	0.13	0.09	0.1
MgO	0.01	1.36	0.99	0.51	1.49	1.71	0.77	0.88
CaO	0.06	4.27	3.67	2.55	4.65	3.91	2.8	3.24
Na ₂ O	1.3	6.87	4.55	5.16	5.78	6	4.63	4.45
K ₂ O	8.28	0.78	3	1.5	2.44	3.59	4.94	4.79
P ₂ O ₅	0.01	0.21	0.41	0.32	0.42	0.35	0.1	0.15
LOI	1.9	2.1	1.4	1.7	1.6	1.4	4	4.9
Total	99.62	99.92	99.95	100.17	99.89	99.81	99.61	100.11
Ba (μg/g)	568	380	1316	1319	1250	1582	1171	1208
Sr	47	872	1235	804	1248	1848	728	762
Zr	707	59	112	77	110	87	96	81
Υ	72	11	20	14	22	20	14	14
	9	10	11	12	13	14	15	16
SiO ₂	61.01	63.77	60.83	66.57	66.04	61.05	74.52	65.37
TiO ₂	0.37	0.27	0.37	0.24	0.25	0.35	0.22	0.38
Al ₂ O ₃	15.91	16.09	15.48	16.44	15.91	17.79	12.71	15.78
Fe ₂ O ₃	3.85	2.74	3.75	1.99	2.15	3.62	2.46	3.93
Cr ₂ O ₃	0	0	0.02	0	0	0	0	0
MnO	0.1	0.09	0.12	0.1	0.09	0.04	0.04	0.11
MgO	0.92	0.47	1.1	0.18	0.27	0.1	0.24	0.6
CaO	3.66	2.8	3.78	2.39	2.86	0.12	0.03	2.73
Na ₂ O	4.51	4.85	4.02	3.58	3.37	0.28	0.12	4.62
K ₂ O	4.89	5.18	4.82	5.12	4.68	14.11	6.58	4.97
P ₂ O ₅	0.14	0.1	0.18	0.06	0.06	0.05	0.04	0.1
LOI	4.5	3.74	5.3	3	3.7	1.3	2.8	0.8
Total	100.08	100.29	99.95	99.84	99.57	99.89	99.91	99.71
Ba (ppm)	1269	1086	1069	1020	1206	1135	1117	1808
Sr	767	720	676	549	522	220	328	1182
Zr	94	102	110	136	155	234	119	206
Υ	14	14	14	14	14	<10	<10	15

1. Aplite sill, Mayflower; 2. Syenite sill, Mayflower; 3. Trachyte, Elkhorn Mountains Volcanics (EMV), Mayflower; 4. Dacite, EMV, Mayflower; 5. Trachyandesite, EMV, Mayflower; 6. Trachyte, EMV, Mayflower; 7. Trachyte, EMV, Mayflower; 8. Trachyte, EMV, Mayflower; 9. Trachyte, EMV, Mayflower; 10. Trachyte, EMV, Mayflower; 11. Trachyandesite, EMV, Mayflower; 12. Crystal Peak quartz monzonite porphyry (near Spotted Horse, Judith Mts; 13. Gold Hill quartz monzonite porphyry (near Spotted Horse, Judith Mts; 14. Gold Hill quartz monzonite porphyry (near Cumberland, Judith Mts; 15. Gold Hill quartz monzonite porphyry (near Mathews, Judith Mts); 16. Big Grassy Peak quartz monzonite porphyry (near Tail Holt, Judith Mts.).

et al. 1997). However, considering the low proportion of pyrite relative to tellurides and other sulphides in stage 3 veins, the contribution of 'invisible gold' to the overall gold budget at Mayflower is likely to be insignificant.

Cocker (1993) reported that tetrahedrite, freibergite $(Ag_6[Ag_6]^{4+})$, $Cu_4C^{2+}_2)Sb_4S_{12}S_{0-1}$, where C is occupied by, for example, Zn, Fe and Cd, and gold-bearing freibergite were present in the Mayflower deposit. Although tetrahedrite, which contains

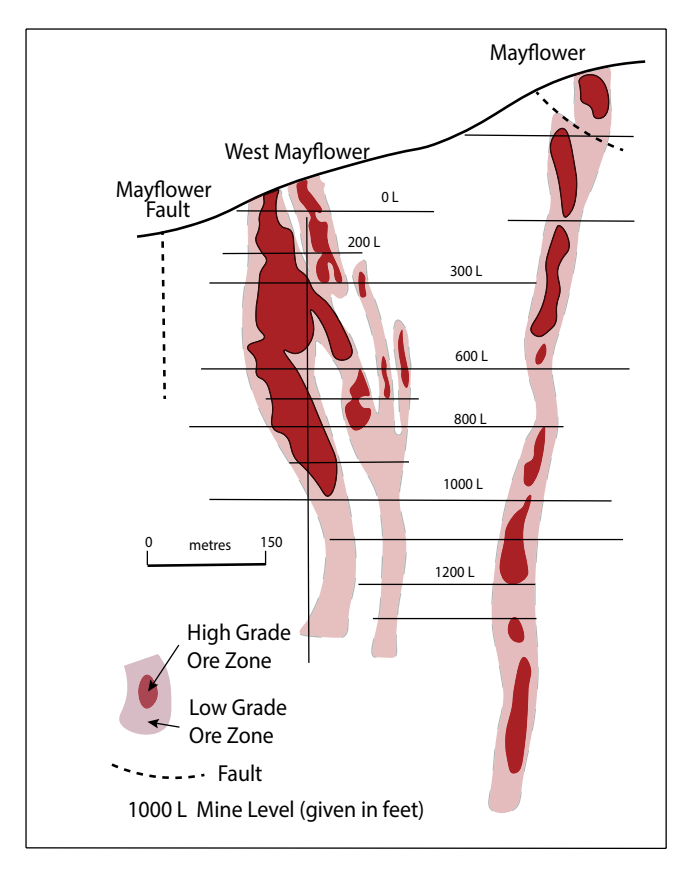


Figure 8. Longitudinal section (see A-A' in Figure 6) through the Mayflower deposit showing the locations of the high- and low-grade ore zones (after Cocker, 1993). The levels indicated are given in feet.

up to 13.0 wt. % Ag (Table 4; Fig. 9), is identified here, the identification of freibergite and gold-rich freibergite remains in doubt due to an absence of compositional data. Tennantite, which is far less common than tetrahedrite, contains considerably smaller amounts of Ag (< 0.45 wt % Ag).

4.c. Judith Mountains deposits

The Judith Mountains are composed of sixteen felsic, porphyritic, laccoliths and stocks of rhyolite, syenite, monzonite, and quartz monzonite that intrude Palaeozoic sedimentary rocks (e.g. Weed & Pirsson, 1897; Woodward, 1995) (Fig. 10). Five types of Late Cretaceous-Early Tertiary deposits are associated with these rocks (Woodward, 1995): 1. Disseminated gold deposits \pm other metals in limestone and skarn; 2. Gold ± silver ± subordinate base metals mainly in veins, shear zones, and stockworks hosted by intrusive rocks and siliclastic rocks; 3. Base metal deposits in Palaeozoic carbonates; and 4. Disseminated copper ± other metals hosted by intrusives. Estimates of up to \sim 20 t Au have been derived from > 90 named and unnamed mines and prospects (Woodward, 1995). Of these gold deposits, the five largest gold telluride deposits are Spotted Horse-Kentucky Favourite (~7.8 t Au), Maginnis (~2.8 t Au), Gies (~1.2 t Au), Cumberland (~1 t Au) and Gilt Edge (~1 t Au). Other deposits that contain possible tellurides include Florence (Get Even), Allen Silver (Silver Dike), Tail Holt and Golden Jack (Woodward, 1995). Non-telluride-bearing Late Cretaceous-Early tertiary base and precious metal deposits spatially related to telluride deposits are also found in the Judith Mountains. Their geological characteristics are summarised in Supplementary Table S1 for comparative purposes.

The Cretaceous-Tertiary intrusive rocks in the Judith Mountains occur along the Cat Creek fault zone, which is one of several W-NW-trending fault zones to form part of the Lewis and Clark Line (Smith, 1965). Kohrt (1991) suggested that the intersection of this lineament with a N-NE-trending structural trend, which parallels the GFTZ may have influenced the emplacement of the alkaline igneous rocks. Kohrt (1991) proposed two periods of Late Cretaceous- to Eocene-age igneous activity in the Judith Mountains: a large volume of calc-alkaline rocks followed by a small volume of alkaline igneous rocks. Radiometric age dating of alkali syenite, tinguaite, alkali granite, rhyolite, hornblende diorite, monzonite, and quartz monzonite using K-Ar, fission track, and U-Th-Pb techniques yields ages ranging from approximately 69 to 47 Ma (Marvin et al. 1980).

The igneous rocks consist of quartz monzonite, monzonite, syenite, diorite, rhyolite, alkali granite, and tinguaite (Weed & Pirsson, 1898; Wallace, 1953, 1956; Zhang & Spry, 1994b; Olinger et al. 2024). Breccias associated with the emplacement of the intrusive rocks are widespread throughout the Judith Mountains and are commonly associated with hydrothermal mineralisation. The composition of five quartz monzonite porphyries obtained herein from the Gold Hill intrusive complex porphyry is given in Table 2 and schematically shown in Figure 3, along with monzonitic rocks and tinguaite porphyries spatially adjacent to the Gies deposit that are given in Zhang and Spry (1994b). Although monzonitic stocks and laccoliths are the most common rock types in the Judith Mountains, rhyolite also occurs as stocks and dykes throughout the Judith Mountains, whereas tinguaite dykes occur predominantly in the eastern part. The presence of inclusions of Precambrian rocks in various intrusions (e.g. Marvin et al. 1980) demonstrates that alkaline igneous rocks intruded the Precambrian basement.

Sedimentary rocks of Cambrian, Devonian, Mississippian, Jurassic, and Cretaceous age, consisting of quartzite, limestone (some of which is fetid), shale, sandstone, mudstone, and siltstone were intruded by the igneous intrusions. The Mission Canyon Limestone and the Lodgepole Limestone of the Mississippian Madison Group host many of the disseminated gold deposits including Giltedge.

Although the geological setting of individual occurrences is described in various degrees of detail in Woodward (1995), the current study focuses on deposits in the Gold Hill mining district (Spotted Horse-Kentucky Favourite, Maginnis, and Cumberland deposits), and the Giltedge and Gies deposits.

4.c.1. Gold Hill mining district

The Gold Hill mining district was the biggest gold producer in the Judith Mountains. The deposits occur on the margins of the Gold Hill intrusive complex in and adjacent to tectonic breccias and Cambrian, Mississippian, and Cretaceous sedimentary rocks (Woodward, 1995). The intrusive complex consists of multiple phases of quartz monzonite porphyry, brecciated blocks of Palaeozoic sedimentary rocks, rhyolite dykes, and tectonic and intrusive breccias, which appear to have been emplaced along faulted contacts with the Crystal Peak and Maiden Peak porphyries.

The most prominent structure in the Judith Mountains is the Warm Springs Fault, which trends N 75° W and has a horizontal displacement of 200 to 300 m. It terminates near the western margin of the Gold Hill porphyry. A northeast-trending set of

Table 3. Representative electron microprobe analyses of tellurium and gold-bearing minerals from the Mayflower deposit

Wt. %*	1	2	3	4	5	6	7
Au	29.12	42.27	25.94	0.00	0.00	0.00	0.00
Ag	9.29	0.74	42.70	59.40	62.11	0.00	0.92
Cu	0.11	0.17	0.00	0.00	0.00	0.01	0.01
Pb	0.00	0.00	0.00	0.00	0.00	61.63	0.00
Hg	0.00	0.00	0.00	0.00	0.00	0.00	58.92
Sb	0.00	0.00	0.00	0.00	0.00	0.00	0.00
Те	61.67	57.64	33.23	40.16	36.75	39.96	40.31
S	0.02	0.00	0.05	0.00	0.00	0.00	0.19
Total	100.23	100.83	100.92	99.56	98.86	101.60	100.35
No. of atoms	6	6	6	6	6	6	6
Au	1.229	1.906	0.992	0.000	0.000	0.000	0.000
Ag	0.716	0.061	2.982	3.818	3.999	0.000	0.078
Cu	0.014	0.024	0.000	0.000	0.000	0.002	0.002
Pb	0.000	0.000	0.000	0.000	0.000	2.922	0.000
Hg	0.000	0.000	0.000	0.000	0.000	0.000	2.712
Sb	0.000	0.000	0.000	0.000	0.000	0.000	0.000
Те	4.018	4.010	1.963	2.182	2.001	3.076	2.915
S	0.028	0.000	0.063	0.000	0.000	0.000	0.292
Wt. %*	8	9	10	11	12	13	14
Au	0.62	9.90	92.82	84.67	73.61	77.65	60.11
Ag	0.30	0.00	7.94	16.24	27.75	22.52	40.72
Cu	0.00	0.00	0.03	0.00	0.00	0.00	0.03
Pb	0.00	55.44	n.a.	n.a.	n.a.	n.a.	n.a.
Hg	0.00	0.00	n.a.	n.a.	n.a.	n.a.	n.a.
Sb	0.00	7.92	n.a.	n.a.	n.a.	n.a.	n.a.
Те	98.77	15.11	n.a.	n.a.	n.a.	n.a.	n.a.
S	0.03	11.33	n.a.	n.a.	n.a.	n.a.	n.a.
Total	99.72	99.70	100.79	100.91	101.35	100.17	100.86
No. of atoms	6	10	1	1	1	1	1
Au	0.024	0.588	0.864	0.741	0.592	0.654	0.551
Ag	0.022	0.000	0.135	0.259	0.408	0.345	0.447
Cu	0.000	0.000	0.001	0.000	0.000	0.000	0.001
Pb	0.000	3.118	n.a.	n.a.	n.a.	n.a.	n.a.
Hg	0.000	0.000	n.a.	n.a.	n.a.	n.a.	n.a.
Sb	0.000	0.747	n.a.	n.a.	n.a.	n.a.	n.a.
Те	5.916	1.375	n.a.	n.a.	n.a.	n.a.	n.a.
S	0.038	4.125	n.a.	n.a.	n.a.	n.a.	n.a.

1 sylvanite (M2A); 2 calaverite (M17544); 3 petzite (9452M); 4 stützite (M2A); 5 hessite (M96-8A); 6 altaite (M95-7); 7 coloradoite (695-10B); 9 nagyagite (605-20B); 10 native gold (17650, stage 3); 11 electrum (17645, stage 5); 12 electrum (17645, stage 5); 12 electrum (17645, stage 5); 14 electrum (17419, stage 5).

faults is very prominent and postdates the Gold Hill porphyry but predates intrusion breccias that form near the end of the intrusive period. These faults appear to have localised ore deposition.

4.c.2. Spotted Horse-Kentucky Favourite

The Spotted Horse-Kentucky Favourite deposits consists of several NNE-trending lodes in a complex zone of Gold Hill quartz-

^{*} Bi, Zn, Fe, As, Sb and Se were also analysed but were not detected in Te-bearing minerals except for nagyagite.

^{*} Zn, Fe, As, Pb, Hg, Te, Se and S were also analysed but were not detected in native gold/electrum.

Table 4. Compositions of sulphosalts and sulphides from Mayflower

		•	•		-	
	1	2	3	4	5	6
Cu	39.13	35.09	37.97	34.23	0.29	0.13
Ag	0.49	6.33	3.03	11.13	0.00	0.04
Fe	0.27	0.39	0.79	3.15	44.38	0.39
Zn	7.78	6.93	7.19	0.49	0.00	66.75
Sb	20.95	18.45	13.66	17.22	0.03	0.01
As	5.02	5.55	11.29	4.85	2.06	0.00
Ві	0.00	0.04	0.00	0.11	0.20	0.09
Te	0.00	0.00	0.04	2.78	0.07	0.01
Se	0.00	0.51	0.00	0.00	0.00	0.00
S	26.18	25.52	26.57	25.21	51.78	33.12
Total	99.82	98.81	100.54	99.17	98.81	100.54
Based on S atoms	13	13	13	13	2	4
Cu	9.805	9.020	9.375	8.908	0.006	0.003
Ag	0.072	0.959	0.441	1.706	0.000	0.001
Fe	0.077	0.114	0.220	0.933	0.982	0.013
Zn	1.894	1.731	1.725	0.124	0.000	1.977
Sb	2.740	2.475	1.855	2.338	0.001	0.002
As	1.894	1.731	2.492	1.070	0.034	0.000
Bi	0.000	0.003	0.000	0.008	0.001	0.001
Te	0.000	0.000	0.005	0.l360	0.001	0.002
Se	0.000	0.106	0.000	0.000	0.000	0.000
S	13.000	13.000	13.000	13.000	2.000	4.000

1 tetrahedrite (16930A); 2 tetrahedrite (M-1); 3 tennantite (697-6F); 4 tetrahedrite (17419); 5 pyrite (17645M); 5 sphalerite (695-75).

monzonite porphyry, Madison Group limestone, polylithic breccias (Fig. 5 g, h), and Cambrian shales and conglomerates (Woodward, 1995). According to R.A. Forrest (unpub. MS thesis, Montana College of Mineral Science and Technology, 1971), limestone replacement bodies, fissure fillings and veins, porphyry replacement, and breccia characterise the gold telluride mineralisation. Roscoelite in a roscoelite-fluorite-quartz-carbonate vein yielded a date of 59.2 to 58.8 ± 2.1 m.y., which probably represents the age of gold-silver telluride mineralisation (Marvin et al. 1980)

Limestone replacement ore averages 110 to 225 g/t Au and is the most important ore type economically. It occurs as disseminations in bleached limestone, fluorite and roscoelite (Fig. 11a). Fissure ore consists of multiple fracture fillings in zones up to 1.5 m wide of veinlets in Palaeozoic sedimentary rocks, whereas porphyry replacement ore is characterised by veinlets in Gold Hill porphyry adjacent to its contact with the Madison limestone. Breccia ore is volumetrically the most important ore type and averages 14 to 40 g/t Au. The breccias consist mostly of fragments of Gold Hill porphyry with lesser amounts of Madison Group limestone (Fig. 5h). It is generally silicified and contain veinlets of kaolinite. In general, the nature of the orebodies is complex and consists of more than one ore type, reflecting deposition at intrusive-sediment contacts and repeated movement along faults.

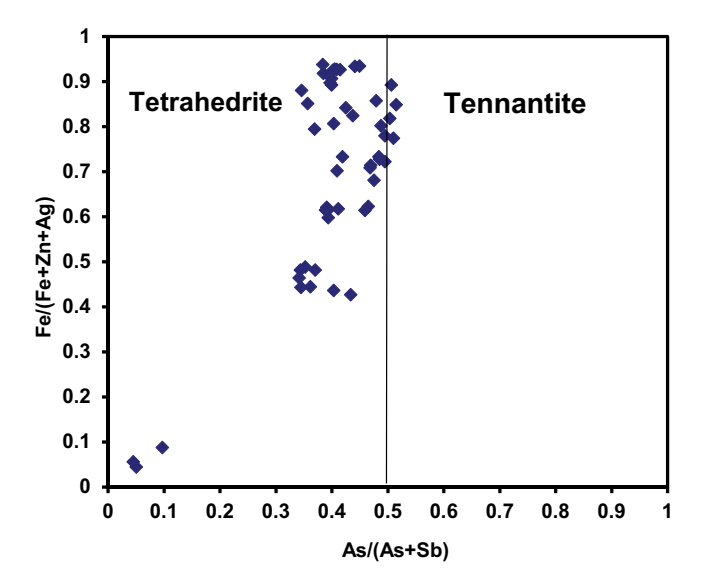


Figure 9. Chemical variation of tetrahedrite–tennantite fahlores from the Mayflower deposit as a function of Fe/(Fe+Zn+Ag) versus As/(As+Sb). Note that tetrahedrite is the predominant fahlores.

Descriptions of the ore mineralisation by Woodward and Giles (1993) and Woodward (1995) suggest that the ore consists of native gold along with sylvanite and petzite. Gold in each of the ore types is spatially associated with fluorite, quartz, calcite, dolomite, pyrite, roscoelite (Fig. 11a), base metal sulphides, adularia and latestage kaolinite. A modified version of the paragenetic sequence of ore deposition determined by R.A. Forrest (unpub. MS thesis, Montana College of Mineral Science and Technology, 1971), incorporates new mineralogical studies undertaken herein (Supplementary Figure S3). Native gold (14.53 to 17.95 wt. % Ag; n = 11) occurs as sponge-like aggregates commonly around pyrite grains or sylvanite-petzite intergrowths and is mostly secondary in origin. Grains of primary gold are rare and, where present, are intergrown with hessite. In addition to sylvanite (8.02 to 9.23 wt. % Ag; n = 28), which is the most common gold-bearing mineral in the Spotted Horse-Kentucky Favourite deposits, other tellurides include petzite and krennerite (3.24 to 7.20 wt. % Ag; n = 7), hessite, and rare altaite. Tellurides are commonly intimately intergrown with roscoelite, sericite, illite and fluorite. Quartz is fine-grained and commonly chalcedonic.

Pyrite exhibits a variety of forms ranging from round fine-grained aggregates disseminated in limestone, subhedral to euhedral grains of variable size (30 µm to 1 mm), pitted anhedral to subhedral grains, rare colloform grains, and aggregates of grains. Tellurides, haematite, sulphides (sphalerite, acanthite (Fig. 11b), galena, chalcopyrite and rare aikinite (PbCuBiS₃), and sulphosalts (tennantite and proustite) occur as inclusions in subhedral to euhedral pyrite. Coarse masses of sphalerite, galena, and chalcopyrite are locally present along with intergrowths of proustite, tennantite, and hessite.

4.c.3. Cumberland and Maginnis deposits

The Cumberland deposit is developed as an E-W-trending vein along the contact between the Gold Hill stock and the Madison Limestone and at the intersection of NE- and NW-trending faults. Gold mineralisation also occurs as disseminations in monzonite porphyry (Corry, 1933). The Maginnis deposit, located ~0.5 km SSW of Cumberland, is primarily located in a brecciated zone up to

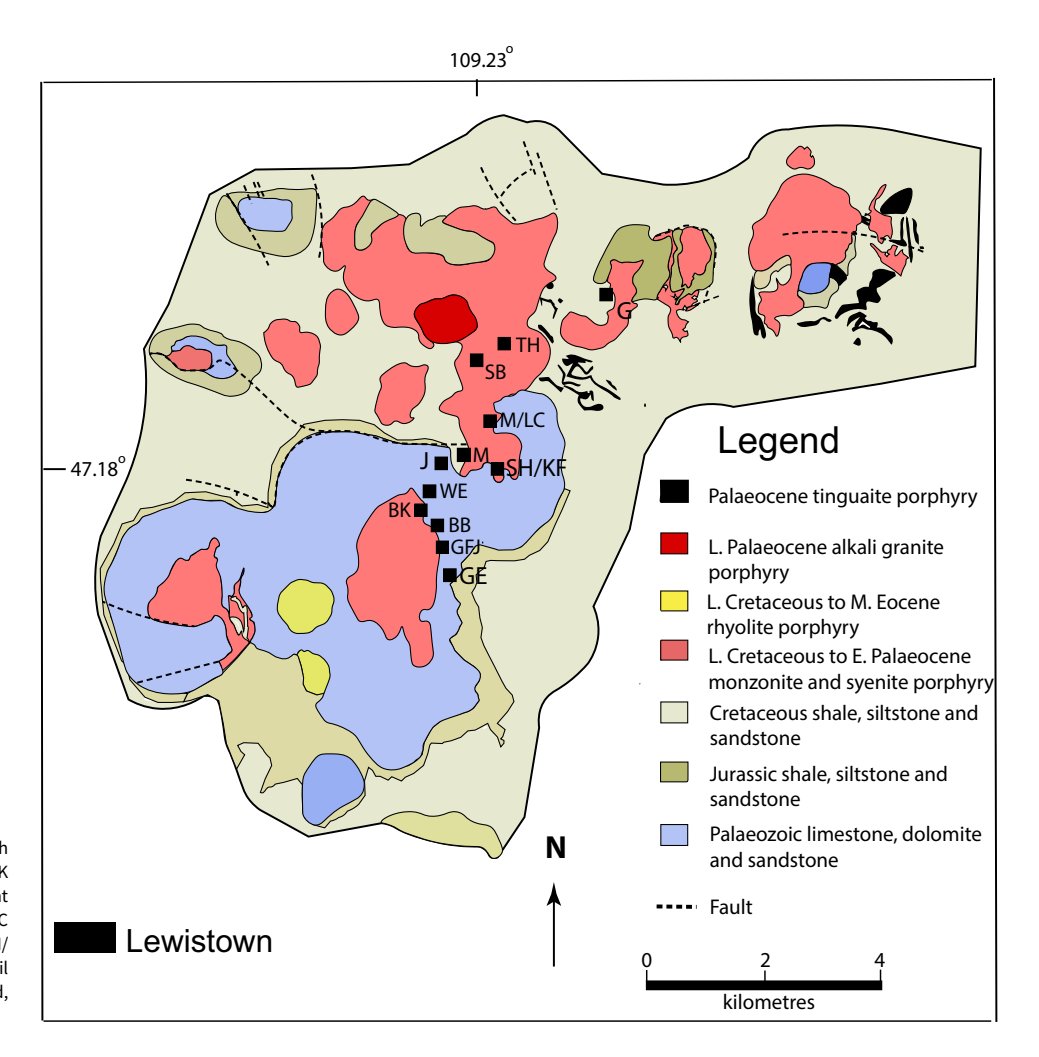


Figure 10. Geologic map of the Judith Mountains. Abbreviations of deposits: BK Butcher Knife, G Gies, GE Gilt Edge, GFJ Great Falls and Judith, J Justice, M Maginnis, M/LC Mathews and Last Chance, SB Silver Bullion, SH/KF Spotted Horse/Kentucky Favourite, TH Tail Holt, WE War Eagle (modified after Woodward, 1995).

1.6 m wide at the contact between monzonite porphyry and silicified limestone of the Madison Group (Woodward, 1995). In addition, Au-bearing replacement bodies also extend a few metres into the limestone. The ore in both deposits contain native gold, sylvanite, fluorite, roscoelite, calcite, kaolinite, and minor pyrite, sphalerite and galena (Woodward, 1995).

4.c.4. Gies deposit

The Gies Au-Ag-Te deposit is an epithermal vein system that occurs along the contact between intrusive rocks of the Cretaceous-Tertiary Elk Creek laccolith (syenite, monzonite porphyry, and monzonite) with the Cretaceous Kootenai Formation (sandstone) (Fig. 12). Tinguaite porphyry dykes (up to 10 m wide and 1.5 km in length) cross-cut these rocks and pre-date and postdate mineralisation. Tellurides are mainly found in two NNW-trending veins that are up to 2 m wide and extend for ~ 500m (Fig. 11c). A second set of veins trends ENE and where it intersects the first set, the highest gold grades are observed, locally as stockworks (Zhang & Spry, 1991, 1994b). The age of mineralisation is unknown, but irregularly distributed alteration is present up to 100 m away from the vein system and consists of silicification and carbonation with potassic alteration, in the form of adularia, occurring within a few metres of the veins. Minor amounts of albitisation and propylitic alteration (chlorite and clinozoisite) are also present.

A four-stage paragenetic sequence was proposed by Zhang and Spry (1994b) and is modified here to incorporate the more recent

mineralogical findings of Spry and Thieben (1996) and Bindi et al. (2006) (Supplementary Figure S4). The mineralogy of the ore veins is complex but is dominated by quartz, roscoelite, pyrite, carbonate (calcite, dolomite, ankerite), sphalerite, and galena. The most prominent mineral assemblages in each stage are (Zhang & Spry, 1994b): stage 1 quartz-pyrite-roscoelite-carbonate; stage 2 quartz-pyrite-base metal sulphides-carbonates-minor telluridesroscoelite; stage 3 quartz-tellurides-pyrite-roscoelite-base metal sulphides-sulphosalts; and stage 4 sulphides-sulphosalts-native gold. Although native gold and electrum are present in stages 3 and 4, precious metal and non-precious metal tellurides as well as native tellurium are most abundant in stages 2 and 3, with minor hessite in stage 4. Sylvanite is the most common telluride in the deposit (Fig. 11d), where it occurs in a variety of assemblages: sylvanite-stützite, sylvanite-altaite-galena ± pyrite, sylvanitehessite, and sylvanite-nagyagite-altaite-galena. Hessite is the most common Ag-rich telluride (Fig. 11e). Other Te-bearing minerals include krennerite, nagyagite, native tellurium, and benleonardite (Supplementary Table S4).

4. d. North Moccasin Mountain deposits (Kendall mining district)

The Kendall mining district (23 t Au at an average grade of ~1.4 g/t) occurs in and on the margins of the highly altered Palaeocene (~66 Ma) North Moccasin Mountains laccolith, a syenite porphyry

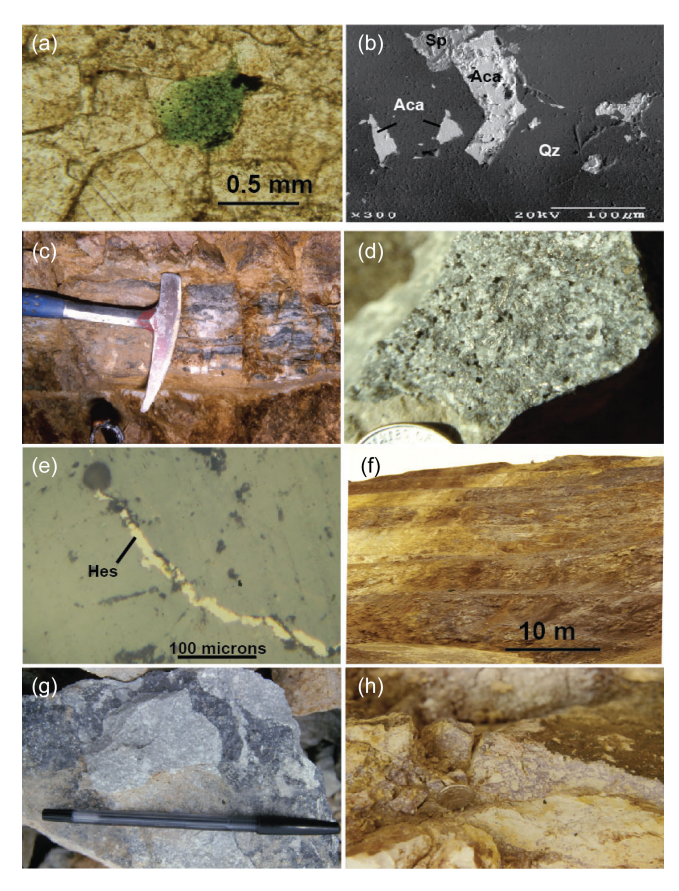


Figure 11. a. Roscoelite grain in recrystallised limestone from the Spotted Horse deposit. b. BSE image of acanthite (Aca) in quartz (Qz) and coexisting with sphalerite (Sp) from the Spotted Horse deposit. c. Quartz-telluride-roscoelite vein from the Gies deposit. d. Sylvanite crystals perched on quartz in a quartz vein, Gies deposit. d. Hessite veinlet in quartz (plane-polarised reflected light image), Gies deposit. e. Oxidized ore zone in the Kendall open-cut pit. f. Sphalerite-pyrite-telluride vein in syenite in the Gold Bug pit, Landusky deposit. g. Brecciated fluorite ore in the Alabama pit, Zortman deposit.

(Ikramuddin et al. 1983, 1986; Lindsey, 1985; Lindsey & Naeser, 1985; Kurisso, 1991; P. Racinet unpub. M.S. thesis, University of Montana, 1994). This laccolith intruded a package of Cambrian to Cretaceous sedimentary rocks (limestone, cherty limestone, dolomite, sandstone, siltstone, black shale, mudstone). Karst breccias occur in the uppermost 85 m of limestone in the Mississippian Madison Group and host the Muleshoe, Horseshoe, Kendall, Cemetery Hill, Plum Creek, Little Dog Creek and Mason Creek deposits (Fig. 13). The first three deposits are the economically most important. The karst breccias are clast-supported and primarily contain fragments of syenite porphyry and limestone, with a fine- to coarse-grained calcite matrix.

The ore zones are oxidised to about 200 m (Fig. 11f). Visible sulphides and gold are largely absent with the metallic minerals consisting of fine-grained arsenian pyrite, native gold, unidentified gold-silver tellurides, and arsenopyrite (Kurisso, 1991). Ikramuddin *et al.* (1983, 1986) pointed out that the ore is enriched in As, Sb, Hg and Tl. Gangue minerals consist of calcite, fluorite, and sooty carbonaceous material, with minor quartz. Alteration is limited, but it is noted here that metallic mineralisation is locally associated with kaolinite, dolomitization, and silicification. Hydrothermal brecciation provided conduits for mineralising fluids, which assisted in karst development and the formation of associated sedimentary collapse breccias.

4.e. Little Rocky Mountain deposits (Zortman-Landusky)

The Zortman (Fig. 14) and Landusky deposits (Fig. 15) contain reserves and resources of ~ 110 t Au with an average grade of 0.54 g/t and a Au/Ag ratio of $\sim 1:7$ (Wilson & Kyser, 1988; Foster & Childs, 1993). Previous studies of the Zortman and Landusky deposits include the geological setting, structure, igneous petrology, hydrothermal alteration, and gold mineralisation (Emmons, 1908; Corry, 1933; Dyson, 1939; Hastings, 1988; Wilson & Kyser, 1988; Ryzak, 1990; Russell, 1991, 1992). Wilson and Kyser (1988) presented isotopic (H, O, S, Ar, Sr, and Nd) and fluid inclusion evidence in concert with field and petrographic data to constrain the age and origin of the intrusive rocks and spatially associated hydrothermal mineralisation.

4.e.1. Geological setting

The regional geological setting of the Little Rocky Mountains is described by Knechtel (1959), Collier and Cathcart (1922), Hastings (1988), Ryzak (1990) and Russell (1991), and only a brief summary is given here. The Little Rocky Mountains consist of Palaeocene syenite, quartz syenite, and quartz monzonite porphyries that intruded Archaean schists and gneisses, and Palaeozoic clastic and carbonate rocks. The composition of very weakly altered igneous rocks obtained by Wilson and Kyser (1988) and Russell (1991) is plotted in Figure 3. Although volumetrically insignificant, trachyte dykes are spatially associated with gold mineralisation particularly in the Landusky deposit. Studies by Knechtel (1959) show that the alkaline igneous rocks intruded a Palaeozoic sequence, which is over 300 m thick of Cambrian sandstone and shale, Ordovician dolomites, and Devonian to Mississippian shales and limestones. Greater than 100 m of Upper Jurassic limestone, glauconitic sandstone, mudstone, and shale (in places carbonaceous) as well as more than 1,200 m of Cretaceous shales, sandstones, conglomerates, and siltstone unconformably overlie the Palaeozoic sequence. The Archaean basement rocks consist of hornblende schists, amphibolites, amphibolite-bearing gneisses, biotite gneisses, quartz-feldspar gneisses, and mafic granofelses (Peterman, 1980; Russell, 1991) and occur in fault contact with the margin of the Palaeocene rocks and as blocks in the intrusive rocks.

4.e.2. Hydrothermal mineralisation and alteration

The Zortman and Landusky deposits are structurally controlled and occur as veins, high-grade stockworks, breccia replacements, and fractured 'sheeted' zones (e.g. Hastings, 1988). Orebodies are typically about 300 m long, 75 m wide, and 150 m deep. Various alkaline porphyritic rocks are associated with mineralisation in both deposits. In the Zortman deposit, mineralisation occurs predominantly at the intersection of north- and northwesttrending fractures, although there is a preferential alignment of orebodies with north-trending faults. Minor mineralisation is aligned in an ENE direction, which parallels the orientation of the Montana lineament (see Fig. 1). Hydromagmatic breccias associated with mineralisation vary from being clast dominant to matrix dominant. Mineralised zones in the Landusky area occur in northeast-trending fracture zones, which parallel the orientation of the GFTZ. Trachyte dykes along zones of mineralisation are characteristic of the Landusky area. Russell (1991) noted that a variant of trachyte, locally referred to as the 'Possum porphyry', possesses a fetid hydrocarbon odour when fractured.

Samples of hydrothermally altered syenite porphyry produced K-Ar dates of 63.9 ± 1.5 to 62.4 ± 1.4 Ma and were considered by

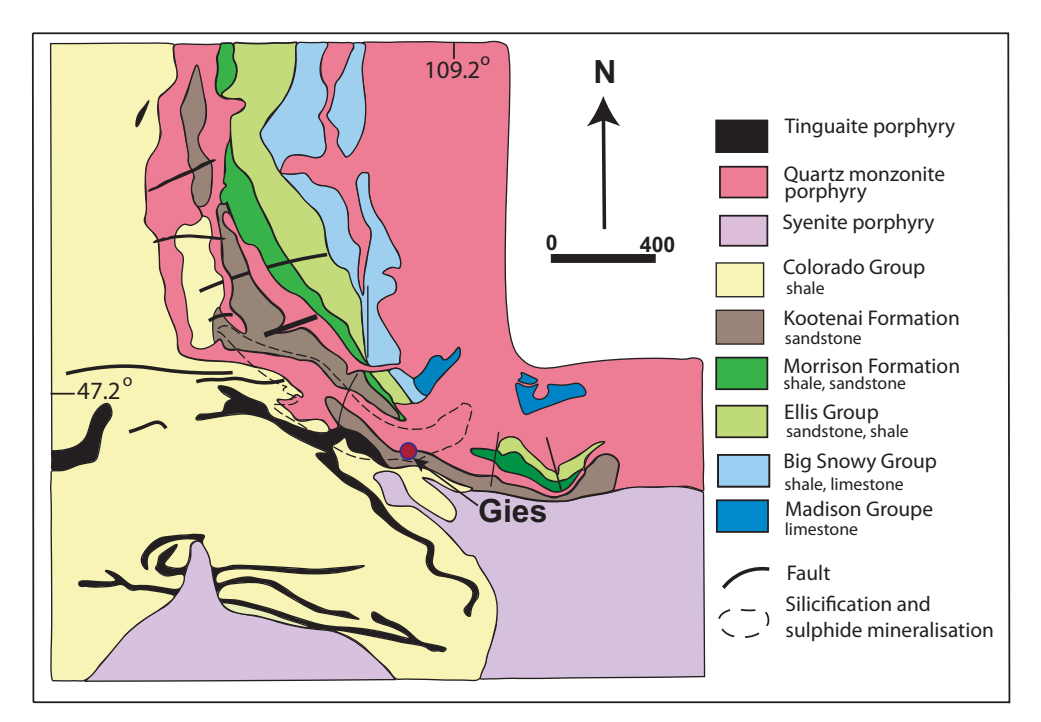


Figure 12. Geological map of the Gies deposit (after Zhang & Spry, 1994b).

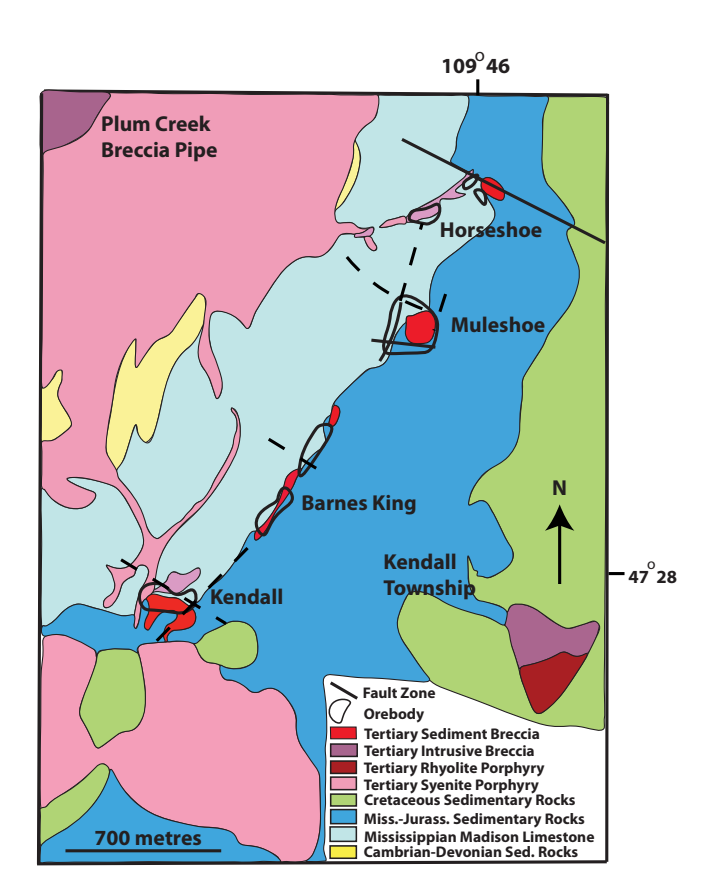


Figure 13. Generalised geological map of the Kendall mine shows individual deposits (after Kurisoo, 1991).

Marvin *et al.* (1980) to date the hydrothermal activity associated with gold mineralisation. These dates are similar to K-Ar dates of 67.8 \pm 16, 62.3 \pm 3, and 57.6 \pm 3 Ma, obtained by Wilson and

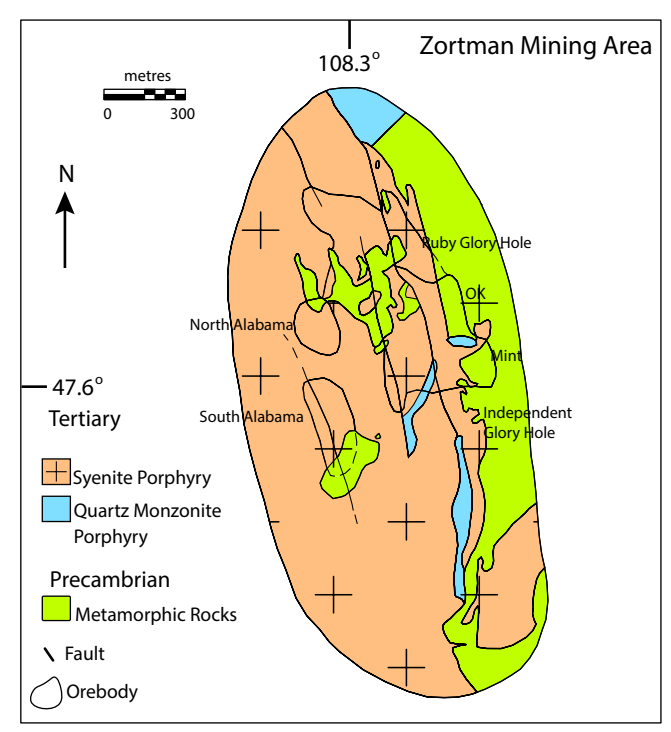


Figure 14. Generalised geological map of the Zortman mine (after Hastings, 1988).

Kyser (1988), which were derived from illite in altered intrusive rocks spatially associated with gold mineralisation.

The upper portions of the mined orebodies are oxidised, whereas zones of sulphides occur below this zone. In the oxidised zones, native gold occurs in fractures with haematite, goethite, and rare jarosite. Based on mineralogical studies herein coupled with previous published studies (e.g. Ryzak, 1990), including

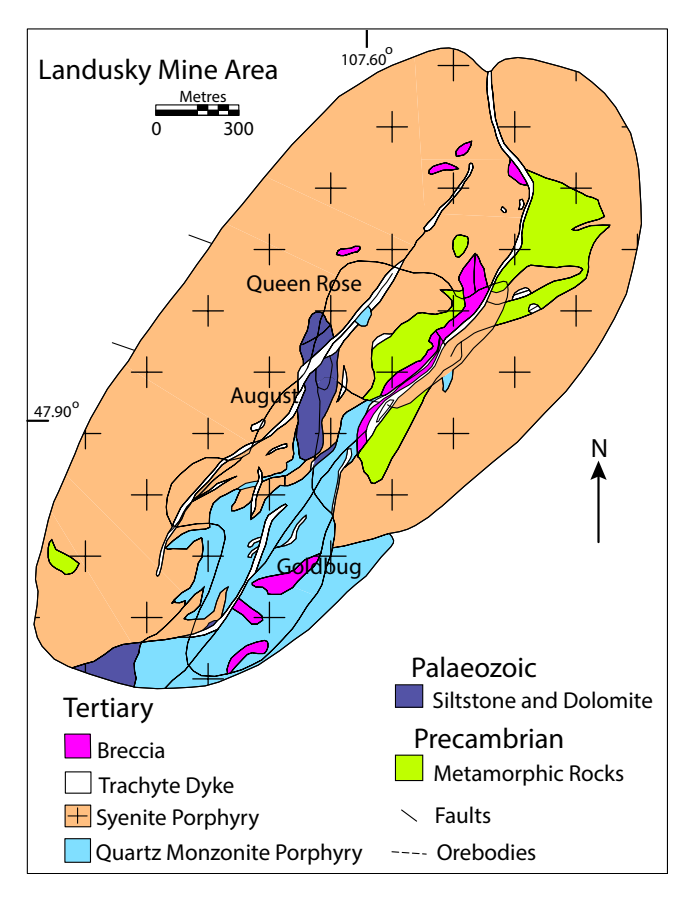


Figure 15. Generalised geological map of the Landusky mine (after Hastings, 1988).

unpublished company reports, we provide a new paragenetic sequence (Supplementary Figure S5). Stage 1 consists of early silicification accompanied by gold-free pyrite, while stage 2 mineralisation is composed of pyrite, marcasite, arsenopyrite, galena, sphalerite (Fig. 11g), chalcopyrite, acanthite and minor amounts of precious metal tellurides and native gold. The coarsest gold grains (up to 120 μ m) occur in this stage. Stage 3 is free of precious metal minerals and is composed primarily of pyrite, marcasite, and arsenopyrite. According to Ryzak (1990), stage 4 mineralisation is the main gold stage, where it occurs as sub-micron gold on the surfaces of pyrite and as tellurides. Minor pyrite and base metal sulphides characterise stage 5, whereas orthoclase flooding, microcline, adularia, quartz veining, and fluorite (Fig. 11h) typify stage 6. It should be noted that reflected studies by us reveal that trace quantities of pyrite, marcasite, chalcopyrite, and rutile in the August pit are intergrown with fluorite and, in places, replace stage 6 fluorite.

Pyrite possesses a variety of forms and textures. Most common is euhedral pyrite that is > 50 μm in size, and occasionally > 2 mm. This form of pyrite is commonly overgrown by aggregate-textured, atoll-textured, or zoned pyrite. In the aggregate-textured pyrite, individual grains are commonly 2 to 6 μm in diameter, whereas pyrite atolls may vary in size from about 10 to 100 μm in diameter. The aggregate texture of pyrite has a pitted or melnikovite appearance where, in places, it is replaced by greigite (Fe₃S₄). A late variety of pyrite is a feather-textured form, which resembles textures described by Murowchick and Barnes (1987) in which pyrite forms as a replacement of marcasite. Note that marcasite

aggregates occur as rims on the early pyrite or as a replacement of euhedral pyrite.

Various Te-bearing minerals have been identified in Zortman-Landusky ores, including calaverite, krennerite, sylvanite, hessite, petzite, empressite, stützite, altaite, coloradoite, melonite, native tellurium, tellurobismuthite, weissite (Cu_{2-x}Te), rickardite (Cu₇Te₅) and an unnamed sulphotelluride of silver (C. Paterson unpub. report to Zortman Mining, 1988; Russell, 1991; R.M. Honea, unpub. reports to Zortman Mining, 1992a, b, c, and d; Supplementary Figure S5). A qualitative scanning electron microscope analysis by R.M. Honea (unpub. report to Zortman Mining, 1992d) of the sulphotelluride suggested a formula of Ag(Te_{0.2-0.4}S_{0.6-0.8}). Although it is unclear which tellurides belong to stage 2 and which formed in stage 4, gold in the form of tellurides is more common at Zortman than Landusky, whereas native gold is more abundant in the Landusky ores. Calaverite, krennerite, sylvanite, stützite, melonite, native tellurium, tellurobismuthite and cervelleite have been reported from the Zortman area only (R.M. Honea, unpub. report to Zortman Mining, 1992d). There are no tellurides that are exclusive to the Landusky area. Silver also occurs as native silver, acanthite, freibergite, polybasite, stromeyerite (AgCuS), jalpaite (Ag₃CuS₂), and the unnamed sulphotelluride.

The most widespread types of alteration are argillic and sericitic, which appear to be spatially linked (Ryzak, 1990; Russell, 1991). Argillic-sericitic alteration affects nearly all intrusive rocks, but some unaltered rocks have been identified. Weak to moderate argillic alteration extends hundreds of metres from orebodies and decreases away from gold mineralisation. Illite, sericite, pyrite, and kaolinite appear to be the most common minerals associated with this style of alteration, however, smectite and leucoxene are also present. Argillic-sericitic alteration manifests itself as a replacement of feldspars and hornblende.

Localised zones of propylitic and potassic alteration along with zones of silicification and fluoritisation are also present (Fig. 11h). The replacement of feldspar by epidote, carbonates and chlorite characterise the propylitic alteration. Although the development of quartz veins is rare, silica and very fine-grained pyrite occur as a replacement of coarse feldspars and groundmass in intrusive porphyritic rocks in and adjacent to gold mineralisation. The silicification of breccias is also common. Opaline silica in open spaces of breccias is locally present (Russell, 1991). Petrographic studies by Russell (1991) showed that potassic alteration is characterized by masses of fine-grained potassium feldspar (20-50 $\mu m)$ that replaced the groundmass and plagioclase phenocrysts of various porphyritic rocks. This style of alteration may be early and associated with the late deuteric/early hydrothermal history of the porphyry system, but the presence of orthoclase flooding along shear zones and adularia in silicified breccias suggests that potassic alteration may have had a protracted history. The presence of late-stage pervasive purple fluorite spatially associated with gold mineralisation is common in and adjacent to the Alabama and Ruby pits of the Zortman area. It occurs as fluorite masses and as a replacement of feldspar phenocrysts and groundmass of brecciated porphyritic rocks (Fig. 11h). Fluorite is rare in the Landusky area.

5. Analytical results

5.a. Sulphur isotope studies

Sulphur isotope compositions were obtained herein from thirtytwo samples of pyrite from the Mayflower ($\delta^{34}S = -29.4$ to

 Table 5.
 Sulphur isotope data from the Mayflower, Zortman-Landusky, and Judith Mountains deposits

Sample no.	Stage/location	Mineral	δ ³⁴ S (‰)	Sample no.	Stage/location	Mineral	δ^{34} S (‰)
Mayflower							
98PS-1 (M)	Stage 1	Ру	- 10.5	98PS-6 (M)	Stage 1	Ру	- 9.2
98PS-7 (M)	Stage 1	Ру	- 4.6	98PS-10 (M)	Stage 1	Ру	- 17.8
98PS-11 (M)	Stage 1	Ру	- 9.9	98PS-13 (WM)	Stage 1	Ру	- 23.9
98PS-14 (WM)	Stage 1	Ру	- 8.1	98PS-18 (WM)	Stage 1	Ру	+ 0.4
98PS-20 (WM)	Stage 1	Ру	+ 1.4	98PS-22 (WM)	Stage 1	Ру	- 21.3
98PS-24 (M)	Stage 1	Ру	- 23.3	98PS-25 (M)	Stage 1	Ру	- 25.5
98PS-26 (M)	Stage 1	Ру	- 24.5	98PS-28 (M)	Stage 1	Ру	- 22.2
98PS-30 (M)	Stage 1	Ру	- 25.2	98PS-31 (M)	Stage 1	Ру	- 26.1
98PS-32A (WM)	Stage 1	Ру	- 19.3	98PS-32B (WM)	Stage 1	Ру	- 15.8
98PS-33 (WM)	Stage 1	Ру	- 19.3	98PS-34 (WM)	Stage 1	Ру	- 21.2
98PS-35 (M)	Stage 1	Ру	- 10.2	98PS-37 (M)	Stage 1	Ру	+ 4.1
98PS-38 (WM)	Stage 1	Ру	- 0.6	98PS-39 (WM)	Stage 1	Ру	- 7.5
98PS-40A (WM)	Stage 1	Ру	- 8.4	98PS-41 (WM)	Stage 1	Ру	- 9.1
98PS-47 (M)	Stage 1	Ру	+ 4.7	98PS-56 (M)	Stage 1	Ру	+ 2.6
98PS-56 (M)	Stage 1	Gn	- 2.5	98PS-60A (M)	Stage 1	Ру	- 29.4
MF97-24 431	Stage 1	Ру	+ 0.3	MFCS #2	Stage 1	Ру	- 5.8
Zortman-Landusky							
695-71 (L)	Gold Bug	Ру	- 7.1	695-85 (Z)	OK	Ру	- 7.0
696-3a (L)	August	Ру	- 0.5	696-3b (L)	August	Ру	- 9.9
696-3c (L)	August	Ру	- 0.4	696-3d (L)	August	Ру	- 3.7
696-3e (L)	August	Ру	+ 1.0	696-3f (L)	August	Ру	- 5.1
696-3g (L)	August	Ру	- 15.0	696-3h (L)	August	Ру	- 3.8
696-3i (L)	August	Ру	- 0.5	696-3m (L)	August	Ру	- 10.8
696-3n (L)	August	Ру	- 4.2	696-3o (L)	August	Ру	- 2.9
696-3p (L)	August	Ру	- 10.2	696-3q (L)	August	Ру	- 5.9
696-3r (L)	August	Ру	- 11.4	696-4 (L)	Queen Rose	Ру	- 9.8
696-5a (L)	August	Ру	- 9.5	696-5e (L)	August	Ру	- 4.4
696-5h (L)	August	Ру	- 10.3				
Judith Mountains							
AMF	American Flag	Gn	- 5.2	GE SFA	Giltedge	Ру	- 20.8
BK-A	Butcher Knife	Gn	- 0.8	ВК-С	Butcher Knife	Gn	- 0.8
9-10-IC #1	Iron Chancellor	Сср	+ 3.0	9-25-GFJ #1a	Great Falls	Sp	- 2.5
9-25-GFJ #1b	Great Falls	Gn	- 4.9	9-26-GFJ #4a	Great Falls	Gn	- 0.7
9-17-WE #2	War Eagle	Gn	- 0.2	9-17-WE #2a	War Eagle	Gn	- 0.3
9-17-WE #2b	War Eagle	Gn	+ 0.9	9-17-WE #4a	War Eagle	Gn	+ 1.7
HGP	War Eagle	Gn	+ 0.8	697-4L	War Eagle	Gn	+ 1.0
697-4R	War Eagle	Gn	+ 0.6	697-1f	Tail Holt	Ру	- 2.4
697-2b	Silver Bullion	Ру	- 0.9	697-3	Justice	Gn	+ 2.3
697-5h	Black Bull	Ру	+ 2.8	697-5q	Black Bull	Ру	+ 3.0
697-16	Mathews	Ру	+ 4.6	697-16	Mathews	Gn	+ 1.7
697-20	Mathews	Ру	+ 4.3	697-20	Mathews	Gn	+ 2.2
697-21	Mathews	Py	+ 3.7	697-21	Mathews	Gn	+ 1.7

(Continued)

Table 5. (Continued)

Sample no.	Stage/location	Mineral	δ ³⁴ S (‰)	Sample no.	Stage/location	Mineral	δ ³⁴ S (‰)
894-26	Spotted Horse	Ру	- 29.9	894-22	Spotted Horse	Ру	+ 6.9
894-40	Gold Hill	Ру	+ 4.5	942-368.5	Kentucky Fav.	Ру	+ 2.9
894-5a	Kentucky Fav.	Sp	+ 2.7	894-5b	Kentucky Fav.	Sp	+ 4.9
894-5c	Kentucky Fav.	Ру	+ 3.2	894-21	Kentucky Fav.	Ру	+ 1.9
942-190	Kentucky Fav.	Ру	+ 8.5				

Abbreviations: Fav. = Favourite, L Landusky, Z Zortman, Ccp chalcopyrite, Gn galena, Py pyrite, Sp sphalerite.

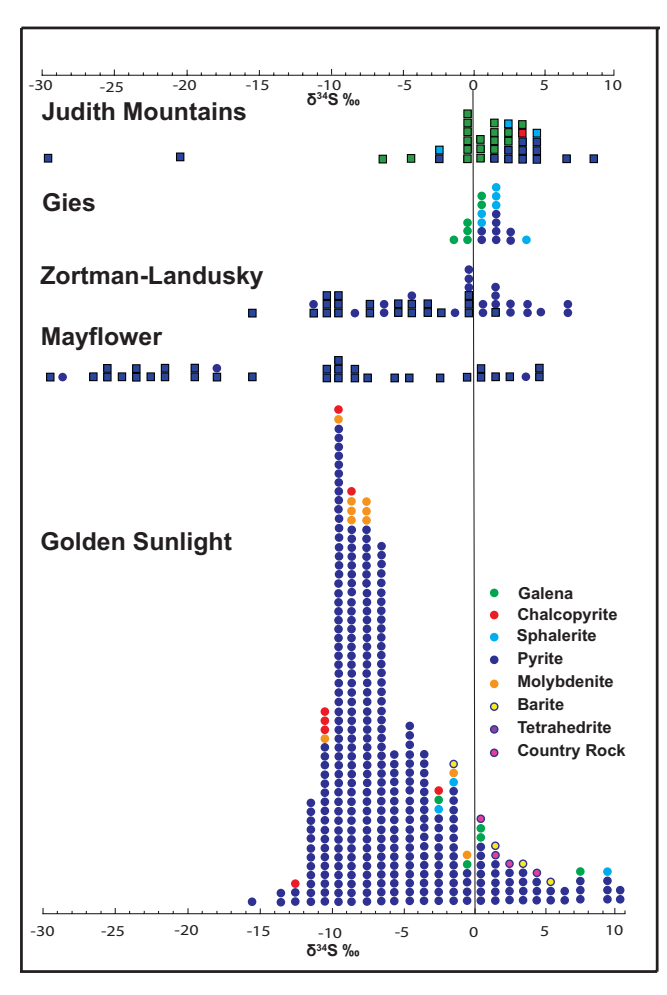


Figure 16. Sulphur isotope compositions of Au-bearing deposits in the Judith Mountains and epithermal Au-Te deposits in central Montana. Data are for the following deposits. a. Judith Mountains (this study); b. Gies (Zhang & Spry, 1994b); c. Zortman-Landusky (Wilson & Kyser, 1977; this study); d. Mayflower (this study) Gammons & Poulson, 2022); and e. Golden Sunlight (Porter & Ripley, 1985; Spry *et al.* 1996; Gammons *et al.* 2020b; Zhao *et al.* 2025). Filled square symbols represent new data collected herein, while filled circles are from previously published studies.

+4.1 ‰; n=17) and West Mayflower ore shoots ($\delta^{34}S = -26.3$ to +1.4 ‰; n=14) and one sample of galena from the Mayflower ore shoot ($\delta^{34}S = -2.5$ ‰) (Table 5; Fig. 16). The study was limited in scope because of the lack of sulphides available that were associated with tellurides. All the pyrite analysed was from the earliest pre-gold stage.

Wilson and Kyser (1988) obtained values of $\delta^{34}S = -6.7$ to +2.6 ‰ (n = 7) for disseminated pyrite in intrusive rocks, -0.9 to 4.1 ‰

(n = 4), disseminated pyrite in quartz-carbonate-fluorite fractures and -11.4 to 6.3 % (n = 10) for massive pyrite in fracture fillings and breccias from the Zortman and Landusky areas. These values are complemented by twenty-one new sulphur isotope values of pyrite obtained herein from fracture and breccia fillings from the August $(\delta^{34}S = -15.0 \text{ to } +1.0; n = 18 \%)$, OK $(\delta^{34}S = -7.8 \%; n = 1)$, Gold Bug $(\delta^{34}S = -7.1 \%; n = 1)$, and Queen Rose pits $(\delta^{34}S = -9.8 \%; n = 1)$ (Table 5; Fig. 16).

Sulphur isotope compositions of sulphides in gold telluride deposits in the Judith Mountains, other than those reported previously for the Gies deposit (Zhang & Spry, 1994b; $\delta^{34}S = -0.4$ to +3.1 ‰; n = 20; with one sample of pyrite from Jurassic Ellis shale yielding δ^{34} S = -15.9 ‰) were analysed here: Spotted Horse-Kentucky Favourite $(\delta^{34}S_{pyrite} = +1.9 \text{ to } +8.5 \text{ } \%, n = 6;$ $\delta^{34}S_{\text{sphalerite}} = +2.7$ ‰, n = 1, with one anomalous sample of pyrite (δ^{34} S = -29.9 %); Tail Holt (δ^{34} S_{pyrite} = -2.4 %; n = 1), and Gilt Edge (δ^{34} S_{pyrite} = -20.8 ‰; n = 1). Twenty five additional sulphur isotope analyses of pyrite (n = 7), galena (n = 16), chalcopyrite (n = 1), and sphalerite (n = 1) were obtained from the following non-telluride deposits for comparative purposes: American Eagle, Black Bull, Butcher Knife, Iron Chancellor, Gold Hill, Great Falls, Justice, Matthews and Last Chance, Silver Bulletin and War Eagle (Table 5, Fig. 16). The compositions range from $\delta^{34}S = -5.2$ to +4.6 % and overlap compositions obtained from gold telluride deposits and three analyses of galena -0.3 ‰, +1.7‰ and +3.0 ‰ for the Spotted Horse, Maginnis, and Mathews and Last Chance deposits reported by Woodward (1995).

5.b. Lead isotope studies

Lead isotopes compositions of seven samples of galena analysed here from the Golden Sunlight deposit (206Pb/204Pb = 18.021- 208 Pb/ 204 Pb = 38.002- 207 Pb/ 204 Pb = 15.574–15.790, 19.105, 39.151; Table 6) plot slightly above or overlap the crustal lead growth curve of Stacey and Kramers (1975) (Fig. 17a and b). They also overlap two whole-rock lead isotope compositions of rhyolite in the Mineral Hill breccia pipe and sedimentary rocks of the Proterozoic LaHood Formation that were obtained by DeWitt *et al.* (1996). Since plutonic rocks in the mine area may be related to the Boulder batholith (DeWitt et al. 1996), Pb isotope compositions of K-feldspar in the Boulder batholith and post-Boulder batholith volcanic rocks (Doe et al. 1968) and intrusive volcanic rocks from Korzeb (2019) have also been included in Figures 17a and b for comparative purposes.

Lead isotope compositions were obtained here from 18 samples of galena in ore deposits from the Judith Mountains (Gies Au-Ag-Te-F-V, n = 6; War Eagle Pb-Zn, n = 5; Great Falls and Judith Pb-Zn-Au, n = 3; Butcher Knife Pb-Zn-Cu-Ag-Au, n = 2; Maginnis Au-Ag-Te-F-V, n = 1; Matthews and Last Chance

Table 6. Lead isotope compositions of galena from the Golden Sunlight deposit and the Judith Mountains

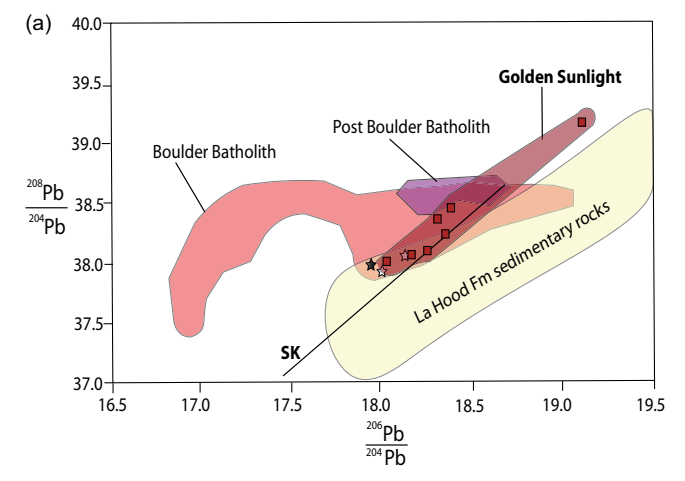
Sample no.	Deposit	²⁰⁶ Pb/ ²⁰⁴ Pb	²⁰⁷ Pb/ ²⁰⁴ Pb	²⁰⁸ Pb/ ²⁰⁴ Pb
PS93-1	Golden Sunlight	19.105 (±0.019)	15.790 (±0.019)	39.151 (±0.019)
PS93-2	Golden Sunlight	18.021 (±0.008)	15.574 (±0.009)	38.002 (±0.009)
PS93-4	Golden Sunlight	18.302 (±0.050)	15.725 (±0.051)	38.356 (±0.052)
PS93-5	Golden Sunlight	18.374 (±0.055)	15.759 (±0.055)	38.447 (±0.055)
PS93-7	Golden Sunlight	18.245 (±0.008)	15.618 (±0.008)	39.090 (±0.009)
PS93-8	Golden Sunlight	18.160 (±0.010)	15.598 (±0.012)	38.052 (±0.012)
697-19b	Golden Sunlight	18.347 (±0.018)	15.651 (±0.017)	38.232 (±0.018)
G-4	Gies	18.829 (±0.039)	15.694 (±0.037)	39.695 (±0.038)
G-5	Gies	18.699 (±0.010)	15.649 (±0.010)	39.367 (±0.010)
90-P5	Gies	18.888 (±0.042)	15.830 (±0.041)	39.815 (±0.041)
90-P16	Gies	18.697 (±0.027)	15.661 (±0.027)	39.298 (±0.027)
90-G2	Gies	18.669 (±0.039)	15.641 (±0.039)	39.214 (±0.039)
90-G8	Gies	18.886 (±0.024)	15.692 (±0.026)	39.398 (±0.026)
697-4	War Eagle	18.358 (±0.008)	15.786 (±0.008)	40.124 (±0.008)
9-17- WE2b	War Eagle	18.240 (±0.008)	15.560 (±0.008)	39.863 (±0.008)
9-17- WE2c	War Eagle	18.269 (±0.008)	15.587 (±0.008)	39.985 (±0.008)
9-17- WE2e	War Eagle	18.669 (±0.010)	15.641 (±0.010)	39.214 (±0.010)
9-17- WE4a	War Eagle	18.407 (±0.011)	15.637 (±0.012)	39.703 (±0.012)
697-3	Great Falls & Judith	19.792 (±0.015)	15.786 (±0.015)	40.033 (±0.016)
9-25- GFJ1b	Great Falls & Judith	18.652 (±0.034)	15.664 (±0.033)	41.007 (±0.033)
9-25- GFJ1c	Great Falls & Judith	18.554 (±0.017)	15.637 (±0.017)	40.786 (±0.016)
BK-A	Butcher Knife	18.052 (±0.052)	15.659 (±0.052)	38.906 (±0.054)
BK-C	Butcher Knife	17.990 (±0.011)	15.602 (±0.012)	38.764 (±0.012)
697-11	Maginnis	19.946 (±0.017)	15.823 (±0.018)	40.325 (±0.018)
MG*	Maginnis	18.53 (±0.19)	15.59 (±0.16)	36.48 (±0.36)
697-21	Mathews & Last Chance	18.859 (±0.018)	15.651 (±0.018)	38.232 (±0.019)
				(Continued)

(Continued)

Table 6. (Continued)

Sample no.	Deposit	²⁰⁶ Pb/ ²⁰⁴ Pb	²⁰⁷ Pb/ ²⁰⁴ Pb	²⁰⁸ Pb/ ²⁰⁴ Pb
LC*	Mathews & Last Chance	19.87 (±0.20)	15.58 (±0.16)	38.33 (±0.38)
SH*	Spotted Horse	18.63 (±0.19)	15.65 (±0.16)	38.14 (±0.38)

^{*} lead isotope data are from Woodward (1995).



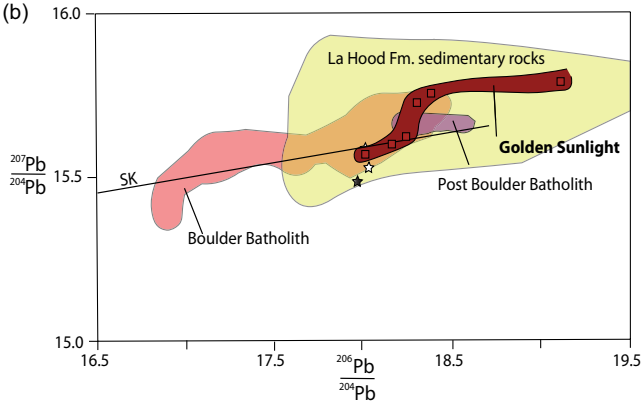
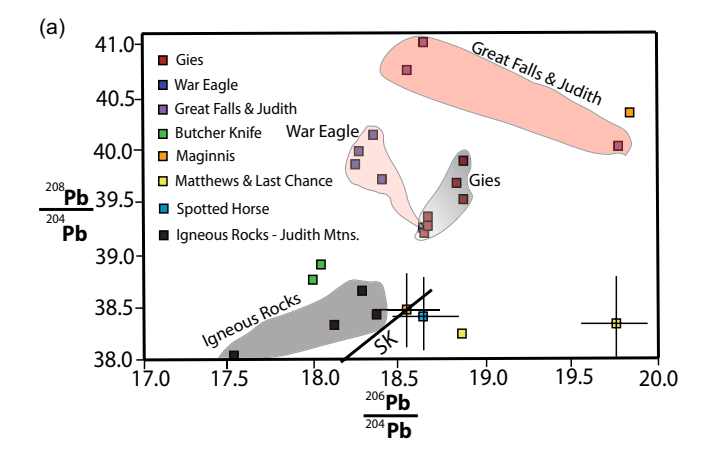


Figure 17. Lead isotopic composition of galena in terms of a. 208 Pb/ 204 Pb versus 206 Pb/ 204 Pb and b. 207 Pb/ 204 Pb versus 206 Pb/ 204 Pb for the Golden Sunlight deposit (this study), whole-rock lead isotope composition of the host rhyolite (shown as open stars) in the Mineral Hill breccia pipe and Proterozoic LaHood sedimentary rocks (DeWitt et al. 1996) as well as a diorite (Korzeb, 2019, shown as a black star). Lead isotopes of K-feldspar in the Boulder batholith and post-Boulder batholith volcanic rocks (Doe et al. 1968) and whole-rock lead isotope compositions of Boulder Batholith granite and intrusive volcanic rocks are from Korzeb (2019).

Pb-Zn-Ag-Au, n=1). It should be noted that the deposits are located in three geographic areas. The Gies deposit is spatially associated with the monzonite-syenite of the Elk Peak laccolith, while the Butcher Knife, War Eagle, and Great Falls and Judith deposits occur on the margins of the Crystal Peak laccolith. Maginnis and Matthews and Last Chance deposits are spatially associated with the Alpine laccolith. Figure 18a and b shows the data, which are listed in Table 6, as functions of 208 Pb/ 204 Pb vs 206 Pb/ 204 Pb and 207 Pb/ 204 Pb vs 206 Pb/ 204 Pb vs 206 Pb/ 204 Pb vs 206 Pb/ 204 Pb (Fig, 18a), most of the data fall above the crustal lead growth curve of Stacey and Kramers (1975). Data



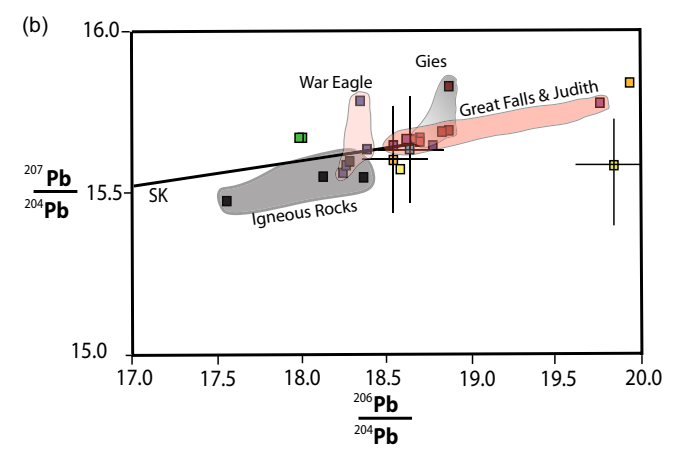


Figure 18. Lead isotopic composition of galena in terms of a. ²⁰⁸Pb/²⁰⁴Pb versus ²⁰⁶Pb/²⁰⁴Pb and b. ²⁰⁷Pb/²⁰⁴Pb versus ²⁰⁶Pb/²⁰⁴Pb for the Butcher Knife, Gies, Great Falls and Judith, Maginnis, Matthews and Last Chance, Spotted Horse and War Eagle deposits. Three samples are from Woodward (1995): Maginnis, Matthews and Last Chance, and Spotted Horse. The error bars on these three samples are an order of magnitude larger than those obtained here, which are within the size of the symbol. The igneous field is derived from Pb isotope analyses of K-feldspar and titanite (Marvin *et al.* 1980).

for the individual deposits generally cluster together, notwith-standing one sample of galena from the Great Falls and Judith deposit, which has a value of $^{206}\text{Pb}/^{204}\text{Pb} = 19.792$ that is considerably higher than the other samples analysed here.

5.c. Fluid inclusion studies

Fluid inclusion studies were conducted previously on the Golden Sunlight (Porter & Ripley, 1985; Spry *et al.* 1996), Gies, (Zhang & Spry, 1994b) and Landusky-Zortman deposits (Wilson & Kyser, 1988; Russell, 1991). To complement these studies, we conducted a preliminary investigation of four samples of stage 1 quartz from the Spotted Horse deposit (Table 7, Fig. 19). The fluid inclusions, which are considered primary given their isolated nature (Roeder, 1984), consist of simple two-phase liquid-vapour inclusions (15–25% vapour). They homogenised into the liquid phase at temperatures (T_h) of 113.3° to 199.6 °C (n = 50) with salinities of 1.1 to 11.9 wt. NaCl equivalent. Eutectic temperatures of -42.0° to -23.8 °C suggest the presence of CaCl₂ as well as NaCl in the oreforming fluid (Oakes *et al.* 1990). The T_h range of secondary inclusions, which occur in crosscutting planes, is lower than the primary inclusions and ranges from 84.7° to 102.0 °C.

5.d. Secondary ion microprobe (SIMS) analyses of pyrite

Secondary ion microprobe analyses of stage 3 pyrite in sample 696-3p from the August pit (Landusky deposit) contain 0.07 to 6.4 μ g/g Au (n=9), whereas marcasite in the same sample contains 0.05 to 0.08 Au μ g/g and 67 to 603 As μ g/g (n=5) (Table 8). SIMS analyses of stage 3 pyrite in sample 695-85 from the OK pit (Zortman deposit) contain 0.06 to 0.44 Au μ g/g and 0.49 to 4,697 As μ g/g (n=13). The data collected herein are probably not representative of the range of gold values observed in pyrite from the Zortman-Landusky deposits, as it was only the coarse euhedral pyrite that was analysed. It is likely that the fine aggregate-textured pyrite contains higher gold and arsenic contents than the coarse variety, in keeping with what has been described elsewhere in the literature (e.g. Simon *et al.* 1999; Spry & Thieben, 2000).

6. Discussion

6.a. Petrography

The compositions of igneous rocks associated with epithermal gold telluride-bearing deposits were determined for the Zortman-Landusky (Wilson & Kyser, 1988; Russell, 1991), Gies (Zhang & Spry, 1994), and Golden Sunlight deposits (DeWitt et al. 1996). In addition, whole rock analyses of intrusive rocks in the Judith Mountains were reported by Wallace (1953), Nockolds (1954) and GL Kirchner (unpub MS thesis Univ of Montana, 1982). To complement these data, whole rock compositions of quartz monzonite porphyries were obtained here from the Spotted Horse, Cumberland, Matthews/Last Chance and Tail Holt deposits in the Judith Mountains (analyses 12-16, Table 2). Trachyte, trachyandesite, syenite and dacite were analysed from the Elkhorn Mountains Volcanics spatially associated with the Mayflower deposit (analyses 1-11, Table 2). The compositions of these rocks and those previously published from epithermal gold telluride deposits in Montana are shown in Figure 3 in terms of $Na_2O + K_2O$ vs SiO_2 and show that most rocks plot in the alkaline field. The quartz monzonite porphyries from the Judith Mountains plot in the alkaline field, while EMV from Mayflower drape the alkaline-subalkaline fields.

6.b. Mineralogy

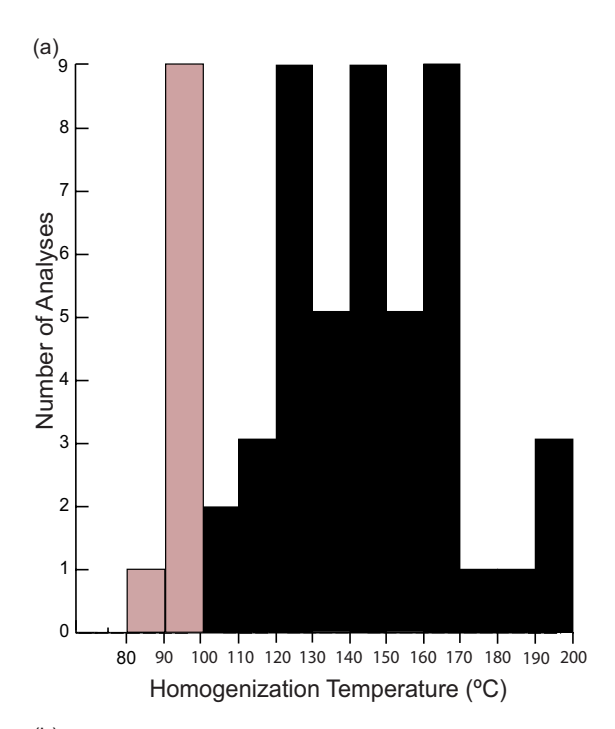
Telluride-bearing deposits in the CMAP consist of a variety of types, including bonanza veins (Gies, Spotted Horse, Mayflower), low-grade carbonate-replacement at igneous rock-carbonate contacts (Kendall, Kentucky Favourite, Gilt Edge), breccia pipehosted (Golden Sunlight) and igneous-hosted (Zortman, Landusky). The mineralogy of the gold-silver telluride deposits is complex, especially in bonanza veins and breccia-hosted ores. In addition to sulphides, Bi sulphosalts, native elements, tellurides, and rare sulphotellurides are also present.

Paragenetic studies show that the precious metal mineralogy varies between deposits (Supplementary Figures S1-S5). Assemblages in the system Au-Ag-Te for the various deposits indicate calaverite is the most common telluride at Golden Sunlight, while sylvanite coexisting with stützite is more prevelant in the Gies deposit, and sylvanite and petzite are the most common tellurides in the Spotted Horse deposit (Fig. 20). Of the deposits studied here, the Mayflower deposit is dominated by the Ag-rich tellurides hessite and stützite, although Au-rich tellurides sylvanite and calaverite are also present. Textural relationships show that Au-rich tellurides generally preceded the formation of the Ag-rich

Table 7. Thermometric data for primary fluid inclusions in quartz from the Spotted Horse deposit

Sample no.	T _{me} (°C)	T _{mf} (°C)	Primary T _h (°C)	Secondary T _h (°C)	Salinity (wt% NaCl equiv.)
894-11A	- 42.0 to - 23.8 (9)	-8.0 to - 1.9 (14)	116.6–174.4 (18)	90.7–101.5 (2)	3.23-11.70
894-1B	- 35.0 to - 24.0 (7)	-7.2 to - 0.6 (10)	115.8–199.6 (25)		1.05-11.93
689-1			113.3-174.7 (5)	90.0-102.0 (7)	
894-11B			123.5–127.1 (2)	84.7-85.0 (4)	

T_{me} eutectic melt, T_{mf} final ice melt, T_h homogenisation temperature (into the liquid phase).



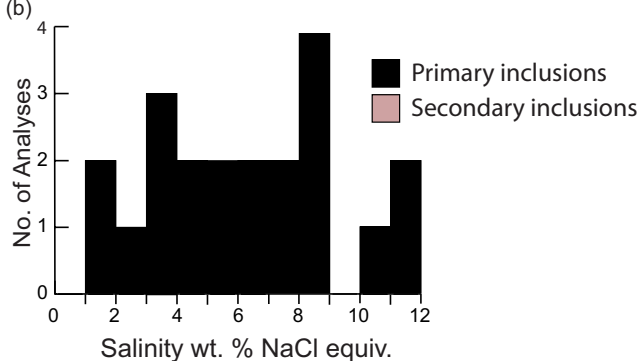


Figure 19. Histograms of a. homogenisation temperature and b. salinities of primary two-phase (liquid-vapour) fluid inclusions in quartz from the Spotted Horse deposit.

tellurides, a feature commonly reported in other epithermal precious metal telluride deposits (e.g. Pals & Spry, 2003; Scherbarth & Spry, 2006). The presence of fluorite and the vanadium mica roscoelite, along with the presence of Bi minerals (e.g. Golden Sunlight, Spotted Horse) and molybdenite (Golden Sunlight, Landusky-Zortman), suggests an elemental signature characterised by Au-Ag-Te±F±V±Bi±Te±Mo for the alkaline igneous rock-related gold telluride deposits.

While precious metals have been reported here as native elements, tellurides, sulphides, and sulphotellurides, it must be noted that Au also occurs as microinclusions in As-bearing pyrite. For example, SIMS analyses of stage I pyrite in the Golden Sunlight deposit by Spry and Thieben (2000) contain up to 0.6 wt. % As and approximately 1 $\mu g/g$ invisible gold. Their calculations showed that invisible gold accounts for about 6-7% of the total gold content of the Golden Sunlight deposit. Similarly, SIMS analyses here of pyrite and marcasite from the Zortman-Landusky deposits contain elevated concentrations of invisible gold (up to 6.4 $\mu g/g$) and As (up to 6,027 $\mu g/g$) (Table 8) A plot of Au vs As (Supplementary Figure S6) shows that there is no systematic relationship between these elements and that concentrations fall well below the solubility limit of gold in pyrite (Reich et al., 2005) suggesting that microinclusions of Au in pyrite are absent.

Furthermore, compositionally zoned pyrite from Mayflower with up to 6 wt. % As in the cores and <0.1 wt. % As in the rims were reported by M.D. Cocker (unpub. report to Anaconda Minerals, 1983). Pyrite with > 2 wt. % As was documented in a stage 3 pyrite (Table 4); As-free pyrites are present in all other stages. Nevertheless, it is apparent that arsenian pyrite spatially associated with the Au-Ag telluride deposits in Montana can also be a significant repository of gold.

6.c. Ore genesis

In a brief review of the geology, mineralogy, and fluid inclusion, and stable isotope characteristics of alkaline igneous rock-related gold telluride deposits of Montana, Thieben and Spry (1995) identified six major ore types: 1. bonanza veins; 2. carbonate replacement at igneous-carbonate contacts; 3. breccia pipe-hosted; 4. igneous-hosted; 5. contact metamorphic (skarns); and 6. sediment-hosted. As Giles (1983) and Thieben and Spry (1995) pointed out, multiple types of ore can occur in any one deposit. For example, at the Golden Sunlight deposit, sulphides occur in Proterozoic sediments, low-grade porphyry molybdenum mineralisation, hydrothermal breccias and auriferous veins (Spry et al. 1996). Similarly, gold telluride mineralisation in the small Spotted Horse-Kentucky Favourite ore system occurs in limestone replacement bodies, fissure fillings and veins, porphyry replacement, and breccias. The Kendall deposit differs from other disseminated gold zones in carbonate rocks in the CMAP in that they are enriched in As, Sb, Hg and Tl along with Au (Ikramuddin et al. 1983, 1986). While resembling Carlin-type Au deposits, mineralisation at Kendall differs in that ore zones also contain anomalous amounts of Te, F and V.

Given the variable geological settings of ore in any given deposit, the ore-forming conditions will also vary for each ore type. Here, we focus on ore-forming conditions for the hydrothermal vein and breccia-hosted ores, which are the dominant telluride-

Table 8. Secondary ion microprobe analyses of Au and As in pyrite and marcasite from the Zortman and Landusky deposits

Sample No. and point analysis	Location	Mineral	As (μg/g)	Au (μg/g)
696-3 (1a)	August pit, Landusky	Pyrite	2,145	0.08
696-3 (1b)	August pit, Landusky	Pyrite	1,453	0.08
696-3 (1c)	August pit, Landusky	Pyrite	3,150	2.8
696-3 (1d)	August pit, Landusky	Pyrite	8,187	0.07
696-3 (3c)	August pit, Landusky	Pyrite	2,051	4.7
696-3 (3d)	August pit, Landusky	Pyrite	3,804	6.4
696-3 (3e)	August pit, Landusky	Pyrite	920	0.09
696-3 (4a)	August pit, Landusky	Pyrite	6,027	0.30
696-3 (4c)	August pit, Landusky	Pyrite	4,201	0.09
696-3 (2a)	August pit, Landusky	Marcasite	145	0.06
696-3 (2b)	August pit, Landusky	Marcasite	202	0.07
696-3 (3a)	August pit, Landusky	Marcasite	67	0.05
696-3 (3b)	August pit, Landusky	Marcasite	176	0.08
696-3 (4b)	August pit, Landusky	Marcasite	603	0.06
696-85 (1a)	OK pit, Zortman	Pyrite	0.49	0.44
696-85 (1b)	OK pit, Zortman	Pyrite	1,965	0.14
696-85 (2a)	OK pit, Zortman	Pyrite	71	0.11
696-85 (2b)	OK pit, Zortman	Pyrite	4,697	0.07
696-85 (3a)	OK pit, Zortman	Pyrite	60	0.08
696-85 (3b)	OK pit, Zortman	Pyrite	79	0.12
696-85 (3c)	OK pit, Zortman	Pyrite	1,375	0.28
696-85 (4a)	OK pit, Zortman	Pyrite	40	0.06
696-85 (4b)	OK pit, Zortman	Pyrite	1.2	0.22
696-85 (5a)	OK pit, Zortman	Pyrite	1,940	0.08
696-85 (5b)	OK pit,	Pyrite	3,574	0.19

(Continued)

Table 8. (Continued)

Sample No. and point analysis	Location	Mineral	As (μg/g)	Au (μg/g)
696-85 (5c)	OK pit, Zortman	Pyrite	321	0.22
696-85 (5d)	OK pit, Zortman	Pyrite	885	0.13

bearing ore types in the CMAP. We have chosen to focus on these ore types because ore-forming conditions are constrained in several deposits via fluid inclusion, stable isotope and radiogenic isotope studies, although the origin of other ore types will also be discussed.

The Golden Sunlight deposit and peripheral mineralisation are the best studied of all the alkaline igneous rock-related gold telluride deposits in Montana. Combining the fluid inclusion studies of Porter and Ripley (1985) and Spry et al. (1996) suggests a broad range of ore-forming temperatures from 145° to 345°C and fluid salinities of 1 to 10 wt. percent NaCl equivalent for the formation of the gold-bearing breccia and vein ore, while the earlier formed quartz-pyrite-K feldspar-molybdenite veins yielded values of T_b, of 132° to 398 °C. These inclusions showed highly variable liquid to vapour ratios and rare three-phase H₂O-CO₂ and multiphase inclusions (one or more daughter crystals), suggesting that these fluids were associated with phase separation (i.e. boiling). Sulphur isotope studies by Porter and Ripley (1985), Spry et al. (1996), Gammons et al. (2020b), and Zhao et al. (2025) show a large range of δ^{34} S values from -15.8 to 11.0 % (Fig.16), with the isotopically sulphur isotope values (> 0 %) being from Proterozoic sedimentary rocks and the isotopically lightest (mostly < 0 ‰) from the porphyry and breccia-pipe hosted ores. A magmatic sulphur contribution to the porphyry and brecciahosted ores was associated with phase separation of a highly oxidised fluid (as indicated by the presence of haematite in oreforming pyrite) whereby fractionation between H₂S and SO₄²- in a cooling magmatic hydrothermal fluid with $SO_4^2 -> H_2S$ accounts for the isotopically light S isotope values (Gammons et al. 2020b). This view is in contrast to that proposed by Zhao et al. (2025), who suggested that H₂S partitioned into the vapour phase and resulted in the broad range of isotopic values of the sulphides. However, the loss of H2S should make the remaining H2S heavier and make it difficult to account for the very light S isotope compositions. He-Ar isotopic studies of fluids in pyrite by Zhao et al. (2025) suggested a mixing of mantle and crustal components to the ore fluid, while O and H isotopic studies by Porter and Ripley (1985) and Spry et al. (1996) are consistent with the mixing of meteoric waters with magmatic fluids during the late stages of ore formation (Fig. 21). Lead isotope studies of galena from Golden Sunlight suggest a crustal source consistent with the origin proposed by DeWitt et al. (1996) for the alkaline igneous rocks in the area (Fig. 17). Although DeWitt et al. (1996) proposed a deep crustal source, our data when plotted on the two lead isotope evolution curves of Zartman and Doe (1981) do not allow for a discrimination between deep and shallow crustal sources (Fig. 22a, b).

The Zortman-Landusky deposits are igneous-hosted (quartz syenite and monzonite) deposits with tellurides occurring in steeply dipping veins and stockworks. Fluid inclusion studies of sphalerite and quartz by Wilson and Kyser (1988) and Russell

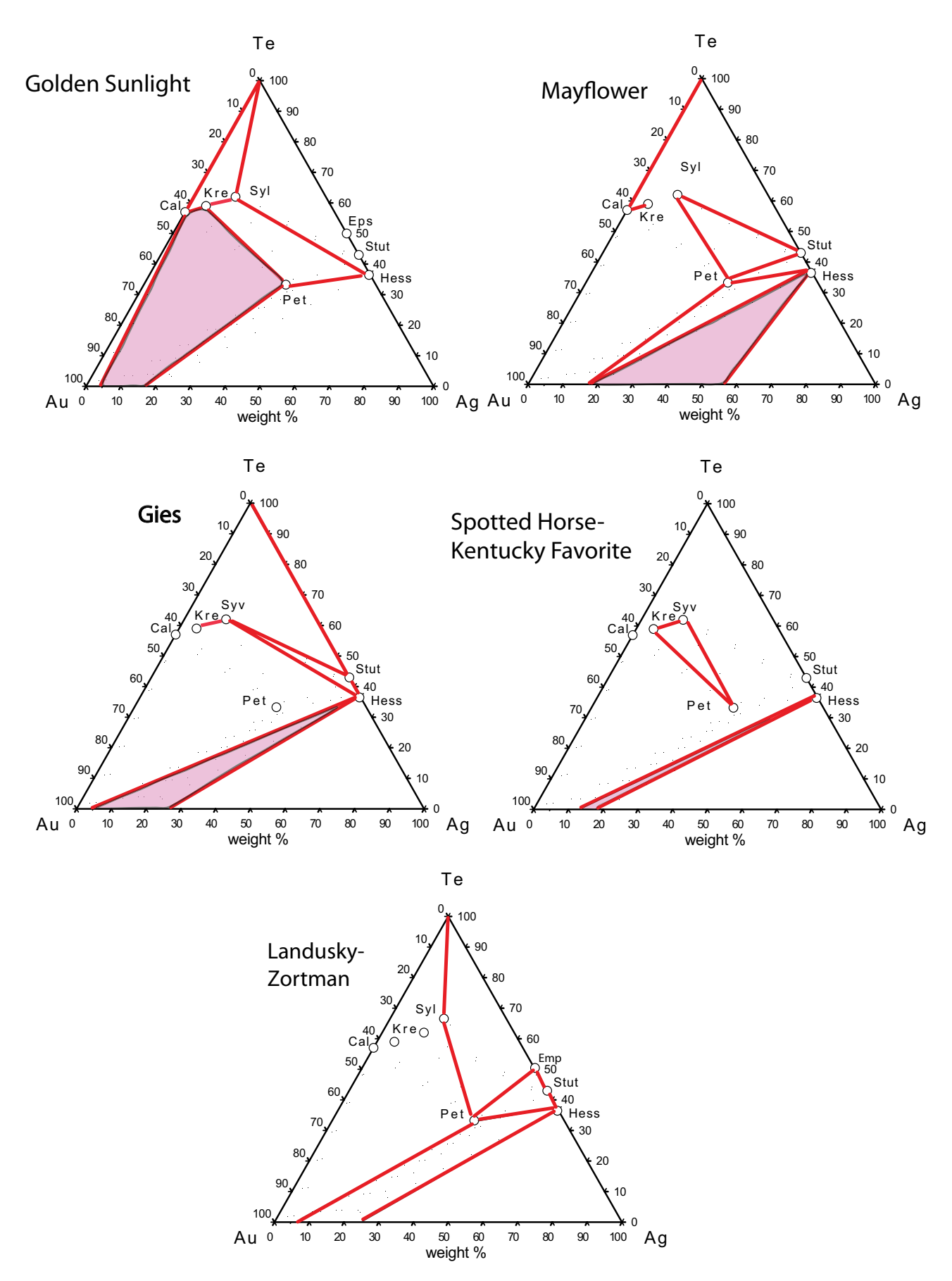


Figure 20. Plot of hydrogen versus oxygen isotope compositions of fluids from Montana Au-Te deposits. Data for the various deposits are: Gies (Zhang & Spry, 1994), Golden Sunlight (Spry et al. 1996), Spotted Horse (this study), Zortman-Landusky (Wilson & Kyser, 1988). Symbols: SH Spotted Horse, SMOW standard mean ocean water.

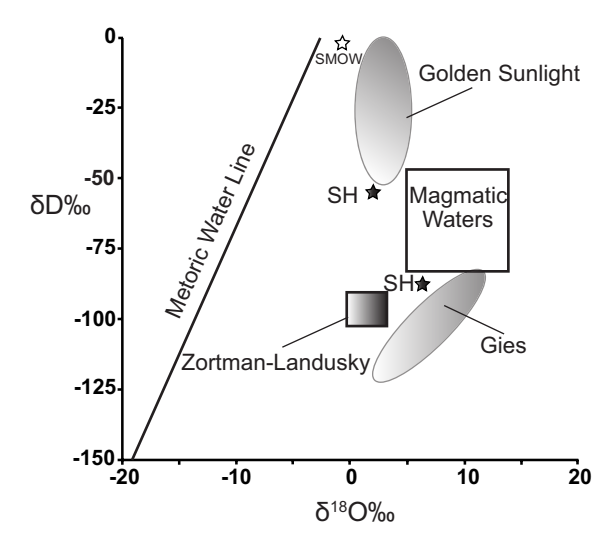


Figure 21. Lead isotopic composition of galena in terms of a. ²⁰⁸Pb/²⁰⁴Pb versus ²⁰⁶Pb/²⁰⁴Pb and b. ²⁰⁷Pb/²⁰⁴Pb versus ²⁰⁶Pb/²⁰⁴Pb for the Butcher Knife, Gies, Great Falls and Judith, Maginnis, Matthews and Last Chance, Spotted Horse and War Eagle deposits. Three samples are from Woodward (1995): Maginnis, Matthews and Last Chance, and Spotted Horse. The error bars on these three samples are an order of magnitude larger than those obtained here, which are within the symbols. Also shown are the Pb isotope evolution curves generated by the plumbotectonics model of Zartman and Doe (1981) for the mantle (A), orogene (B), upper crust contributed to the orogene (C), and lower crust contributed to the orogene (D).

(1991), respectively, suggest the ore-forming fluids boiled between 240° and 340 °C with later non-boiling fluids in fluorite forming at lower temperatures (110° to 200 °C). These latter inclusions exhibited salinities between 0.5 and 3.5 equiv wt percent NaCl.

On the basis of mass balance equations, Wilson and Kyser (1988) argued that oxygen and hydrogen isotope data for illite, which they considered to be the alteration product most intimately associated with pyrite and gold, was most consistent with the interaction of a meteoric ore fluid with the Precambrian gneisses at Landusky (Fig. 21). They noted that the only scenario in which the ore fluid could have interacted with the intrusive rocks is at very low water/rock ratios (i.e. <0.01). Wilson and Kyser (1988) proposed that further support for the involvement of the ore fluid with the basement gneisses was provided by Sr isotope data. Strontium isotope ratios of whole rock samples and feldspar separates from the intrusive rocks have ⁸⁷Sr/⁸⁶Sr ratios of 0.7043 to 0.7061, whereas a single sample of Lodgepole limestone has a ⁸⁷Sr/ ⁸⁶Sr ratio of 0.7081. These values are low by comparison to ratios obtained from Precambrian gneisses (0.7104 to 0.7646) by Peterman (1980) and for illite (0.7168 to 0.7784), when corrected to an age of 60 Ma, which were derived by Wilson and Kyser (1988) for the age of the mineralization. Later formed fluorite and dolomite have values of 0.7070 to 0.7090, which appear to have been derived from a source with much lower 87Sr/86Sr ratios, such as the Palaeozoic limestones and the Cretaceous-Tertiary intrusive rocks.

Wilson and Kyser (1988) argued that the wide range of sulphur isotope compositions of sulphur was derived from mixing of igneous, sedimentary, and metamorphic sources. Combining Wilson and Kyser's (1988) data from fracture fillings and breccias with those obtained in the present study from the same rock types yields a range of δ^{34} S values of -15.0 to +6.3% (Fig. 16). Although this range is greater than the narrow range of disseminated pyrite in spatially associated intrusive rocks (-6.7 to +4.0%), it is likely that there is a source of sulphur other than the intrusive rocks. Since no data were obtained from disseminated sulphides in the

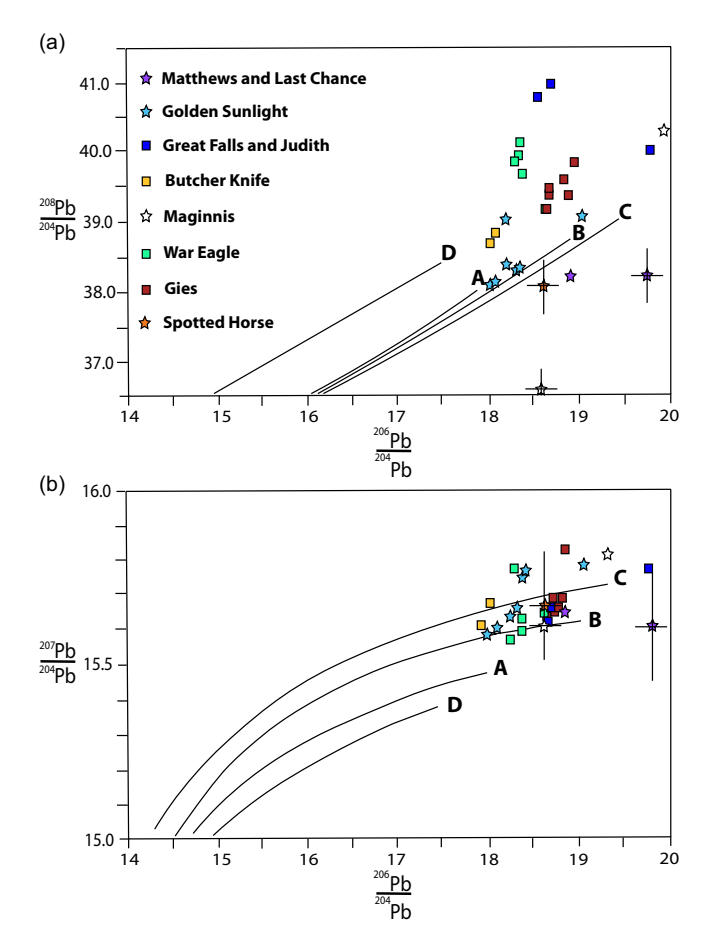


Figure 22. Ternary plots of members in the system Au-Ag-Te showing precious metal assemblages for the various gold telluride deposits in Montana: Golden Sunlight, Mayflower, Gies, Spotted Horse-Kentucky, Landusky-Zortman. Details of the assemblages for each deposit is given in the text.

Precambrian basement, it is unclear whether it contributed sulphur to the ore fluids. One possibility is a contribution of biogenic sulphur from the Palaeozoic sedimentary rocks. Such a source would explain the light sulphur isotope compositions and the wide range of isotopic values. To this end, it is significant to note that gilsonite, black carbonaceous material, was reported by Knechtel (1959) in vugs in the Mission Canyon limestone near Landusky and in vugs in quartz monzonite porphyry 50 m north of the old Goldbug mine. Knechtel (1959) proposed that the gilsonite represented carbonaceous material that migrated into the porphyry from the enclosing Palaeozoic sedimentary rocks. However, given that most of the pyrite analysed in the current study yields negative sulphur isotope values and that the oreforming was likely boiling, raises the possibility that, like the oreforming fluids associated with the Golden Sunlight deposit, the ore fluid possessed a high SO_4^2 -/ H_2S ratio with H_2S partitioning into the vapour phase. However, the oxidised nature of the ore fluid remains in doubt, given the absence of sulphates and the rarity of haematite (just present in stage 4, Supplementary Figure S5), making this scenario less likely.

For deposits in the Judith Mountains, fluid inclusion data from Spotted Horse (this study) and the Gies deposit (Zhang & Spry 1994) suggest that gold was deposited from non-boiling fluids. Mean primary fluid inclusion temperatures for three quartz-bearing stages (1, 2 and 3) at the Gies deposit decreased from $293^{\circ} \pm 10^{\circ}$ C, to $256^{\circ} \pm 9^{\circ}$ C and then to $220^{\circ} \pm 13^{\circ}$ C), respectively.

These temperatures are higher than the homogenisation temperatures (113.3° to 199.6 °C) in quartz from the Spotted Horse deposit (Fig. 19). Oxygen and hydrogen isotope compositions of waters from the Gies and Spotted Horse deposits (Zhang & Spry, 1994; Thieben & Spry, 1995), like those from the Golden Sunlight deposit, support the concept of a mixing of magmatic and meteoric fluids during the precipitation of gold tellurides (Fig. 21). Lead isotope studies of galena in the Judith Mountains (Fig. 18) show that the data occur beyond the 0 age of Stacey and Kramers (1975) and do not overlap the Pb isotope compositions of igneous rocks in the Judith Mountains, which occur below their crustal growth curve. The Pb isotope data for deposits in the Judith Mountains are radiogenic, suggesting interaction with sedimentary rocks through which the ore-forming fluids passed. Regardless of the source of Pb, our data do not allow discrimination of crustal sources based on the orogene arrays of Zartman and Doe (1981) (Fig. 22 a, b).

In the absence of fluid inclusion, radiogenic and O-H isotope data, we largely rely on the mineralogy and sulphur isotope compositions to help determine the conditions of formation of the Mayflower deposit. The presence of coexisting sylvanite and petzite in veins implies, on the basis of the experimental data of Cabri (1965), a maximum temperature of formation of these Te-bearing minerals of 170°C. However, it is possible that these higher temperature phases may have reequilibrated to lower temperatures upon cooling. The range of δ^{34} S values of sulphides in the deposit is large (-29.4 to +4.1 %). The possible sources of sulphur and the reasons for the large isotopic variation are: 1. Biogenic reduction of seawater sulphate; 2. Boiling of the ore fluid, which will result in the loss of H₂S and produce an increase in fO₂ and result in significant variations in the isotopic composition of precipitating sulphides; and 3. Inorganic reduction of seawater sulphate near the pyrite-haematite boundary. The biogenic reduction of seawater sulphate is a viable reason for the wide range of sulphur isotope values. A major part of the Jefferson Dolomite is a thinly bedded, coarsely crystalline fetid dolomite. According to Cocker (1993), 'hydrocarbons occur in films on individual grains and in tiny interstitial pellets'. The circulation of hydrothermal fluids through the fetid dolomite could result in highly variable isotopic values. However, given the absence of sulphur isotope compositions of S-bearing species in the Jefferson Formation, this hypothesis remains speculative. The question of whether boiling was an important process in the deposition of ore mineralization at Mayflower also remains uncertain because of the lack of direct evidence for the process. The absence of lattice-textured bladed calcite, which is commonly ascribed to boiling (e.g. Simmons & Christenson, 1994), and the lack of transparent minerals for fluid inclusion studies hinder efforts to determine whether or not the ore mineralisation was deposited from a boiling hydrothermal fluid. Nonetheless, high dissolved gas contents of ore fluids can extend the depth of first boiling (Hedenquist & Henley, 1985), which Cooke et al. (1996) proposed was the reason for the large vertical extent (> 700m) of precious metal mineralisation in the Baguio district. Although there is no direct evidence for high dissolved gas contents of the ore-forming fluid at Mayflower, this may account for the large vertical extent (> 400 m) of gold-silver mineralisation at Mayflower. However, variations in temperatures and pressures of the ore fluid could also produce phase separation. Negative sulphur isotope values are consistent with sulphide precipitation under oxidising conditions (e.g. near the pyrite-haematite boundary where large variations in the ratio ΣSO₄/ΣH₂S are expected). However, the only members of the system Fe-S-O present at Mayflower are pyrite and marcasite. Haematite is notably absent, even as inclusions in pyrite, which is a common feature of ores elsewhere in the CMAP, including the nearby Golden Sunlight deposit.

7. Comparisons with other alkaline igneous rock-related gold telluride deposits

Alkaline-igneous rock-related gold telluride deposits occur in rocks of Mesozoic to Neogene age (Kelley et al. 2020). Most of the largest deposits are low-sulphidation (adularia-sericite) epithermal deposits, similar to those in Montana. Worldwide deposits occur as veins (e.g. Emperor, Pals & Spry, 2003), breccia-fillings and disseminations (e.g. Cripple Creek, Kelley et al. 1998; Kadel-Harder et al. 2021) and may be genetically related to low-grade porphyry Mo or Cu deposits (e.g. Emperor, Cripple Creek). They occur in various geological settings, including post-subduction or back-arc rifts and continent-arc collision zones (e.g. Richards, 1995; Kelley et al. 2020). They are spatially related to deep structures that allow for the upwelling of magmatic-hydrothermal fluids and alkaline magmas. This also appears to be the case for the location of alkaline igneous rock centres in Montana that are spatially related to the regional NE-SW trending Great Falls Tectonic Zone and the NW-SE trending Lewis and Clark Line (Fig. 1), the latter of which is a prominent zone of oblique-slip, dipslip and strike-slip faults (Sears et al. 2010). Host rocks are varied and include monzonite, quartz monzonite, monzogranite, diorite, syenite, phonolite, and lamprophyre. While the alkaline-igneous rock-related gold deposits contain varying proportions of native metals, sulphides, sulphosalts, tellurides and sulphotellurides, they also commonly contain adularia, sericite, carbonates, fluorite, and roscoelite (e.g. Emperor and Tuvatu, Fiji; Pals & Spry, 2003; Scherbarth & Spry, 2006). These ores have the following characteristic elemental signature: Au-Ag-Te-F-V, which is part of the elemental signature recognised for deposits in central Montana (e.g. Golden Sunlight, Spotted Horse, Gies).

In summarising the results of fluid inclusion studies, Kelley et al. (2020) showed that homogenisation temperatures in various minerals in worldwide gold telluride deposits range from ~80° to 350 °C with most reported salinities ranging from 0.5 to 10 wt. percent NaCl. The telluride-bearing stages primarily occur between 130° and 270 °C, which is commensurate with the range of temperatures derived from fluid inclusion studies for minerals in gold telluride deposits in Montana, with similar fluid salinities. In some deposits, metallic mineral precipitation is associated with phase separation (e.g. Tuvatu, Golden Sunlight). Similar to the gold telluride deposits in Montana, oxygen and hydrogen isotope studies suggest a magmatic contribution with meteoric waters (and possibly evolved groundwater) associated with ore formation (e.g. Emperor and Tuvatu, Fiji; Pals & Spry, 2003; Scherbarth & Spry, 2006). Sulphur isotopes also indicate magmatic values for most gold telluride deposits worldwide, including those in Montana, although a sedimentary contribution is also indicated for some deposits (e.g. Emperor, Ahmad et al. 1987; Mayflower, Zortman-Landusky). Lead and noble gas isotopic constraints (He, Ne, Ar) of Te-bearing low sulphidation precious metal deposits in NE China point to the derivation of ore fluids from mafic magmas from the mantle and mixing with meteoric waters at shallow levels (e.g. Zhai et al 2015; Gao et al. 2024). Lead isotope studies of alkaline igneous rock-related deposits in Montana (Golden Sunlight, Gies, Spotted Horse, Maginnis) suggest the involvement of crustal Pb in a manner similar to that proposed by Kelley et al.

(1998) for Cripple Creek, Colorado. While Te and Au can be carried in the vapour and liquid phases under varying physicochemical conditions (e.g. Williams-Jones & Heinrich, 2008; Zhu et al. 2011; Grundler et al. 2013; Zhai et al. 2018; Hurtig et al. 2025), it is also apparent that immiscible polymetallic Te-Au-rich melts may interact with hydrothermal fluids and result in the precipitation of telluride-rich gold ores (e.g. Jian et al 2021; Fan et al. 2025). Experimental studies of Cabri (1965) showed that the eutectic in the system Au-Ag-Te is 304 °C while Fan et al. (2025) showed that it can be as low as 243° to 270 °C due to the presence of minor elements including Ag, Pb, Bi, Cu, Fe and S in the melt. The system Au-Bi has a eutectic at 241 °C (Nathans & Leider, 1962; Okamoto & Massalski, 1983), suggesting, in the case of the Golden Sunlight deposit, where Gammons and Singh (2024) identified polymineral inclusions in high-grade calaverite-tetradymite ore and proposed that they are melt inclusions. Fluid inclusions in quartz with homogenisation temperatures as high as 398 °C (Spry et al. 1996) are well above eutectic temperatures in this system. The elemental association Au-Bi-Te-Cu-S is also characteristic of metallic mineral assemblages in the Zortman and Spotted Horse-Kentucky Favourite deposits and raises the possibility that polymetallic Te-bearing melts may have formed elsewhere in the central Montana alkali belt.

8. Conclusions

The major conclusions of the present study are as follows:

- 1. Epithermal gold telluride deposits in the CMAP of Montana are spatially related to alkaline igneous rocks (monzonite, quartz monzonite, diorite, syenite, tinguaite, and lamprophyre) that upwelled along regional faults within the Great Falls Tectonic Zone and the Lewis and Clark Line.
- Metallic mineralisation exhibits a variety of types, including: low-grade carbonate-replacement zones at igneous rock contacts, bonanza veins, breccia pipe-hosted deposits, igneous-hosted and disseminations, with multiple types occurring at any given location.
- 3. The deposits are characterised by a complex metallic mineralogy involving tellurides, sulphotellurides, sulphides and native elements with Au:Ag ratios from <4 to 20, and an adularia-sericite±roscoelite±fluorite alteration.
- 4. An elemental signature of Au-Ag-Te±F±V±Mo can be used for exploration purposes for both Au and Ag, as well as the critical element Te, and resembles the elemental association for other worldwide alkaline igneous rock-related epithermal deposits. Gold telluride mineralisation in hydrothermal breccias at Golden Sunlight is telescoped on a low-grade porphyry Mo system while molybdenite occurs in the igneous-hosted Zortman-Landusky deposits.
- 5. Mineralogical, paragenetic and O and H isotope data suggest that gold-silver tellurides generally formed late in the paragenetic sequence of multiple stages of hydrothermal mineralisation from meteoric fluids that were preceded by fluids with a magmatic component. Metallic minerals were precipitated from fairly oxidised, moderately saline, and near-neutral pH fluids at around 130° to 270 °C. Although the source of sulphur is considered to be magmatic in most deposits, a sedimentary contribution from disseminated sulphides related in spatially Palaeozoic Palaeoproterozoic sedimentary rocks may also be important in some deposits in Montana. The deposits that are associated

- with a boiling fluid commonly have negative sulphur isotope values, suggesting fractionation between $\rm H_2S$ and $\rm SO_4^{2-}$ in a cooling magmatic-hydrothermal fluid. Lead isotopes are commensurate with a crustal source of Pb.
- 6. The presence of bonanza-grade ores in some deposits (e.g. Golden Sunlight, Spotted Horse-Kentucky Favourite) may be the result of the precipitation of Au and Te from a boiling fluid or to the interaction between an immiscible polymetallic melt and ore fluids under epithermal conditions.
- 7. Epithermal gold telluride deposits in the CMAP share geological and geochemical characteristics with alkaline igneous rock-related Au-Te deposits elsewhere in the world (e.g. Cripple Creek, Ladolam, Porgera, Emperor, Tuvatu) in that they are commonly associated with upwelling alkaline magmas spatially related to major structures, hydrothermal breccias and, in the case of the Golden Sunlight deposit, is spatially related to a porphyry system. The Au-Ag-Te±F±V hydrothermal signature generally related to alkaline igneous rock-related Au-Te deposits worldwide is also recognised in the CMAP deposits.

Supplementary material. To view supplementary material for this article, please visit https://doi.org/10.1017/S0016756825100290

Acknowledgements. We would sincerely like to thank Allan Kirk for allowing us access to the Mayflower property and for discussions concerning the geology of the Mayflower deposit. Dick Berg and Lester Zeihen, formerly of the Montana Bureau of Mines, are gratefully acknowledged for kindly providing samples from the Mayflower deposit, as is Mark Cocker, who furnished us with additional samples and sections. Richard Forrest provided sulphide samples from some occurrences in the Judith Mountains for sulphur isotope studies. Alfred Kracher aided with electron microprobe analyses. Bruce Nelson (University of Washington) analysed lead isotope compositions, while sulphur isotope compositions were determined by Doug Crowe (University of Georgia) and Ed Ripley (Indiana University). Various discussions with Fess Foster, Taras Bryndzia, Tom Chadwick, Jack Truckle, David Odt, and Chris Gammons improved our understanding of the geology of the Golden Sunlight deposit. The constructive reviews of Chris Gammons and an anonymous reviewer are greatly appreciated and significantly improved the quality of the manuscript. Tim Johnson is thanked for his editorial handling of the paper and for his comments.

Competing interests. The authors declare none.

References

Ahmad M, Solomon M and Walshe JJ (1987) Mineralogical and geochemical studies of the Emperor gold telluride deposit, Fiji. *Economic Geology* **82**, 345–70.

Baker DW (1992) Central Montana alkalic province: Critical review of Laramide plate tectonic models that extract alkalic magmas from abnormally thick Precambrian lithospheric mantle. Northwest Geology 20/21, 71–95.

Bindi L, Spry PG and Pratesi G (2006) Lenaite, AgFeS₂, from the Gies gold-silver telluride deposit, Judith Mountains, Montana, U.S.A.: Composition, physical properties and determination of the crystal structure. *Canadian Mineralogist* **44**, 207–12.

Bird P (1998) Kinematic history of the Laramide orogeny in latitudes 35°-49°N, western United States. *Tectonics* 17, 780–801.

Boerner DE, Craven JA, Kurtz RD, Ross GM and Jones FW (1998) The Great Falls tectonic zone: suture or intracontinental shear zone? *Canadian Journal of Earth Sciences* **35**, 175–83.

Cabri LJ (1965) Phase relations in the Au-Ag-Te system and their mineralogical significance. *Economic Geology* 60, 1569–606.

Cabri LJ, Rowland JF, Gilles LaFlamme JH and Stewart JM (1979) Keithconnite, tellurpalladinite and other Pd-Pt tellurides from the Stillwater Complex, Montana. *Canadian Mineralogist* 17, 589–94.

Childs JF and Foster F (1993) A geologic summary of significant lode gold systems in Montana. Society for Mining Metallurgy and Exploration Preprint 93–244, 40pp.

- Chryssoulis SL, Cabri LJ and Lennard W (1989) Calibration of the ion microprobe for quantitative trace precious metal analyses of ore minerals. *Economic Geology* **84**, 1684–90.
- Cocker MD (1993) Primary dispersion patterns in a carbonate-hosted, epithermal, high-grade Au-Ag telluride system: Mayflower mine, Madison County, Montana, USA. *Journal of Geochemical Exploration* 47, 377–90.
- Collier AJ and Cathcart SH (1922) Possibility of finding oil in laccolithic domes south of the Little Rocky Mountains, Montana. U.S. Geological Survey Bulletin 736-F, 171-8.
- Cooke DR, McPhail DC and Bloom MS (1996) Epithermal gold mineralization, Acupan, Baguio district, Philippines: geology, mineralization, alteration, and thermochemical environment of ore deposition. *Economic Geology* 91, 243–72.
- Corry AV (1933) Some gold deposits in Broadwater, Beaverhead, Phillips, and Fergus counties, Montana. Montana Bureau of Mines and Geology Memoir 10, 162.
- DeWitt E, Foord EE, Zartman RE, Pearson RC and Foster F (1996) Chronology of Late Cretaceous igneous and hydrothermal events at Golden Sunlight gold-silver breccia pipe, southwestern Montana. U.S. Geological Survey Bulletin 2155, 48pp.
- Doe BR, Tilling RI, Hedge CE and Klepper MR (1968) Lead and strontium isotope studies of the Boulder Batholith, southwestern Montana. *Economic Geology* **63**, 884–906.
- Donovan JJ, Rivers ML and Armstrong JT (1992) PRSUPR: automation and analysis software for wavelength dispersive electron-beam microanalysis on a PC. American Mineralogist 77, 444–5.
- Dyson JL (1939) Ruby Gulch gold mining district, Little Rocky Mountains, Montana. Economic Geology 34, 201–13.
- Eggler DH and Furlong KP (1991) Petrochemical and geophysical evidence for old mantle lithosphere beneath. Montana. In *Guidebook to the Central Montana Alkalic Province; Geology, Ore Deposits and Origin* (eds DW Baker and RB Berg), pp. 87–91. Montana Bureau of Mines and Geology Special Publication 100.
- Eggler DH, Meen JK, Welt F, Dudas FO, Furlong KP, McCallum ME and Carlson RW (1988) Tectonomagmatism of the Wyoming province. *Colorado School of Mines Quarterly* 83, 24–40.
- Emmons WH (1908) Gold deposits of the Little Rocky Mountains, Montana. U.S. Geological Survey Bulletin 340, 96–116.
- Fan G-H, Li J-W, Zhong R-C, Gleeson SA, Yao Z-S, Harlov DE, Deng X-D, Cui H, Yu C and Gao W-S (2025) Polymetallic Te-rich melts contribute to efficient enrichment and precipitation of Au in hydrothermal ore deposits. *Geochimica et Cosmochimica Acta* https://doi.org/10.1016/j.gca.2025.03.027.
- Fier NE (1992) Beal Mountain gold deposits, mine geology, and exploration. Northwest Mining Association 98th Annual Meeting, Spokane Washington, 25 pp.
- Foster F and Childs JF (1993) An overview of significant lode gold systems in Montana, and their regional geologic setting. Exploration and Mining Geology 2, 217–44.
- Gammons CH, Gnanou H, Odt D and Poulson SR (2020b) Mineralogy and sulfur isotope geochemistry of polymetallic, porphyry-epithermal mineralization peripheral to the Golden Sunlight gold mine, Montana. *Ore Geology Reviews* 126, 103797.
- Gammons CH, Korzeb S and Hargrave P (2020a) Metallic ore deposits of Montana. In Geology of Montana—Special Topics (eds J Metesh and CH Gammons), Montana Bureau of Mines Special Publication 122, 2, 30 pp.
- Gammons CH, Mosolf J and Poulson SR (2019) Precious metal mineralogy, S-isotopes, and a new LA-ICP-MS date for the Easton and Pacific lode mines, Virginia City district, Montana. Montana Bureau of Mines Special Publication 120, 91–100.
- **Gammons CH and Poulson SR** (2022) A review (with new data) of S-isotopes in hydrothermal mineral deposits of Montana. *Montana Bureau of Mines Special Publication* **123**, 125–30.
- Gammons CH and Singh J (2024) Petrography of a box of high-grade, gold-telluride drill core from the Golden Sunlight Mine. Montana Bureau of Mines Special Publication 124, 33–40.

- Gao S, Hofstra AH, Qin K, Zou X, Pribil MJ, Hunt AG, Manning AH, Lowers HA and Xu H (2024) Lead and noble gas isotopic constraints on the origin of Te-bearing adularia-sericite epithermal Au-Ag deposits in a calc-alkaline magmatic arc, NE China. American Mineralogist 109, 1717–37.
- Giles DH (1983) Gold mineralization in the laccolith complexes of central Montana. In The Genesis of Rocky Mountain Ore Deposits: Changes with Time and Tectonics (ed JW Babcock), pp. 157–62: Proceedings of the Denver Region Exploration Geologists Society symposium.
- Giletti BJ (1966) Isotopic ages from southwestern Montana. *Journal of Geophysical Research*, 71, 4029–36.
- Goddard EN (1988) Geologic map of the Judith Mountains, Fergus County, Montana. U.S. Geological Survey Miscellaneous Investigation Series Map I-1729.
- Grundler PV, Brugger J, Etschmann B, Helm L, Liu W, Spry PG, Tian Y, Testemale D and Pring A (2013) Speciation of aqueous tellurium (IV) in hydrothermal solutions and vapors and the role of oxidized tellurium species in gold metallogenesis. *Geochimica et Cosmochimica Acta* 120, 298–325.
- Hanson AM (1952) Cambrian stratigraphy in southwestern Montana. Montana Bureau of Mines and Geology Memoir 33, 46pp.
- Hastings JS and Harrold JL (1988) Geology of the Beal gold depsoit, German Gulch, Montana. In Bulk Mineable Precious Metal Deposits of the Western United States (eds RW Schafer, JJ Cooper and PG Vikre), pp 207–220.
- Hastings JS (1988) Gold deposits of Zortman-Landusky, Little Rocky Mountains, Montana. In Bulk Mineable Precious Metal Deposits of the Western United States (eds RW Schafer, JJ Cooper and PG Vikre), pp. 187–205. Reno, Nevada: Geological Society of Nevada.
- **Hedenquist JW and Henley RW** (1985) The importance of CO₂ on freezing point measurements of fluid inclusions; evidence from active geothermal systems and implications for epithermal ore deposition. *Economic Geology* **80**, 1379–406.
- Hurtig NC, Adams JR, Marion L, Slodczyk A, Gysi AP and Midisov AA (2025) Te and Au mobility at the porphyry-epithermal transition: Insights from experiments and numerical simulations. 18th SGA Biennial Meeting 2025, Golden Colorado. Abstract 146.
- Ikramuddin M, Asmeron Y, Nordstrom PM, Kinart KP, Martin WM, Digby SJ and Afemari AA (1983) Thallium: a potential guide to mineral deposits. *Journal of Geochemical Exploration* 19, 465–90.
- **Ikramuddin M, Besse L and Nordstrom PM** (1986) Thallium in the Carlintype gold deposits. *Applied Geochemistry* **1**, 493–502.
- Irvine TN and Baragar WRA (1971) A guide to the chemical classification of the common volcanic rocks. *Canadian Journal of Earth Sciences* 8, 523–48.
- **Jensen EP and Barton MD** (2000) Gold deposits related to alkaline magmatism. *Reviews in Economic Geology* **13**, 279–314.
- Jian W, Mau J, Lehmann B, Cook NJ, Xie G, Liu P, Duan C, Alles J and Niu Z (2021) Au-Ag-Te rich melt inclusions in hydrothermal quartz veins, Xiaoqinling lode gold district, central China. *Economic Geology* 116, 1239–48.
- Johnson TW and Meinert LD (1994) Au-Cu-Ag skarn and replacement mineralization in the McLaren deposit, New World district, Park County, Montana. *Economic Geology* 89, 969–93.
- Kadel-Harder IM, Spry PG, Layton-Mathews D, Voinot A, von der Handt A and McCombs AL (2021) Paragenetic relationships between low and highgrade gold mineralization in the Cripple Creek Au-Te deposit, Colorado: trace element studies of pyrite. Ore Geology Reviews 127, 103847.
- **Kelley KD and Ludington S** (2002) Cripple Creek and other alkaline-related gold deposits in the southern Rocky Mountains, USA: influence of regional tectonics. *Mineralium Deposita* **37**, 38–60.
- Kelley KD, Romberger SB, Beaty DW, Pontius JA, Snee LW, Stein HJ and Thompson TB (1998) Geochemical and geochronological constraints on the genesis of Au-Te deposits at Cripple Creek, Colorado. *Economic Geology* 93, 981–1012.
- Kelley KD and Spry PG (2016) Critical metals associated with alkaline-rock related epithermal gold deposits. Reviews in Economic Geology 18, 195–216.
- Kelley KD, Spry PG, McLemore VT, Fey DL and Anderson ED (2020) Alkalic-type epithermal gold deposit model. U.S. Geological Survey Scientific Investigations Report 2010-5070-R, 74 pp.
- Kelly WC and Goddard EN (1969) Telluride ores of Boulder County, Colorado. *Geological Society of America Memoir* 109, 237pp.

- Kiilsgaard TH and Lewis RS (1985) Plutonic rocks of Cretaceous age and faults in the Atlanta lobe of the Idaho Batholith, Challis Quadrangle. U.S. Geological Survey Bulletin 1658 A-S, 29-42.
- Kleinkopf MD (1991) Regional geophysical investigations of the central Montana alkalic province. In *Guidebook to the Central Montana Alkalic Province; Geology, Ore Deposits and Origin* (eds DW Baker and RB Berg), pp. 131–32. Butte, MT: Montana Bureau of Mines and Geology Special Publication 100.
- Knechtel MM (1959) Stratigraphy of the Little Rocky Mountains and encircling foothills, Montana. U.S. Geological Survey Bulletin 1072-N, 723–49.
- Kohrt PB (1991) Alkalic rocks of the Judith Mountains, central Montana. In Guidebook to the Central Montana Alkalic Province; Geology, Ore Deposits and Origin (eds. DW Baker and RB Berg), pp. 77–85. Butte, MT: Montana Bureau of Mines and Geology Special Publication 100.
- Korzeb SL (2019) Interpretation of new and previous lead isotopic data for Late Cretaceous to Eocene satellite intrusions, Butte Granite, Volcanic rocks, and base metal veins of the Boulder Batholith, southwestern Montana. *Montana Bureau of Mines and Geology Bulletin* 139, 40 p.
- Kurisoo P (1991) Gold deposits of the Kendall mining district, Fergus County, Montana. In Guidebook to the Central Montana Alkalic Province; Geology, Ore Deposits and Origin (eds DW Baker and RB Berg), pp. 39–44. Butte, MT: Montana Bureau of Mines and Geology Special Publication 100.
- Lageson DR, Kalakay TJ and Foster DA (2020) Mountain building: The orogenic evolution of Montana. In Geology of Montana, Volume 1— Geologic History (eds JJ Metesh and SM Vuke), pp. 1–65. Butte, MT: Montana Bureau of Mines and Geology Special Publication 122.
- Larsen ES (1940) Petrographic province of central Montana. Geological Society of America Bulletin 51, 887–948.
- Le Bas MJ, Le Maitre RW, Streckeisen A and Zenettin B (1986) A chemical classification of volcanic rocks based on the total alkali-silica diagram. *Journal of Petrology* 27, 745–50.
- Lindsey DA (1985) A gold-mineralized breccia zone at Kendall, North Moccasin Miuntains, Fergus County, Montana. United States Geological Survey Professional Paper 1301-C, 45–55.
- Lindsey DA and Naeser CW (1985) Relation between igneous intrusion and gold mineralization in the North Moccasin Mountains, Fergus County, Montana. United States Geological Survey Professional Paper 1301-B, 37-44.
- Lochman-Balk C (1971) The Cambrian of the craton of the United States. In Cambrian of the New World (ed CH Holland), pp. 79–167, Wiley-Interscience New York.
- Lund K and Aleinikoff JN (2022) Temporal relations between the Boulder Batholith and Elkhorn Mountains Volcanics, western Montana: "The Nature of Batholiths" revised. Montana Mining and Mineral Symposium: Technical Papers: Montana Bureau of Mines and Geology Special Paper 123, 89–97.
- Marvin RF, Hearn BC Jr, Mehnert HH, Naeser CW, Zartman RE and Lindsey DA (1980) Late Cretaceous-Paleocene-Eocene igneous activity in north-central Montana. *Isochron/West* 29, 5–25.
- McCallum IS, Thurber MW, O'Brien HE and Nelson BK (1999) Lead isotopes in sulides from the Stillwater Complex, Montana: evidence for subsolidus remobilization. Contributions to Mineralogy and Petrology 137, 206–19.
- McMannis WJ (1965) Resumé of depositional and structural history of western Montana. American Association of Petroleum Geologists Bulletin 49, 1801–23.
- McNulty BA and Jowitt SM (2022) Byproduct critical metal supply and demand and implications for the energy transition: A case study of tellurium supply and CdTe PV demand. Renewable and Sustainable Energy Reviews 168, 112838.
- Moyle AL, Doyle BJ, Hoogvliet H and Ware AR (1990) Ladolam gold deposit, Lihir Island. Australian Institute of Mining and Metallurgy Monograph Series 14, 1793–805.
- Mueller PA, Heatherington AL, Kelly DM, Wooden JL and Mogk DW (2002)Paleoproterozoic crust within the Great Falls tectonic zone: Implications for the assembly of southern Laurentia. *Geology* 30, 127–30.
- Murowchick JB and Barnes HL (1987) Effects of temperature and degree of supersaturation on pyrite morphology. *American Mineralogist* 72, 1241–50.
- Mutschler FE, Griffen ME, Stevens DS and Shannon SS Jr (1985) Precious metal deposits related to alkaline rocks in the North American Cordillera,

- and interpretive review. Transactions of the Geological Society of South Africa 88, 355-77
- Mutschler FE, Johnson DC and Mooney TC (1991) A speculative kinematic model for the central Montana alkalic province and related gold deposits. In Guidebook to the Central Montana Alkalic Province; Geology, Ore Deposits and Origin. (eds DW Baker and RB Berg), pp. 121–8. Butte, MT: Montana Bureau of Mines and Geology Special Publication 100.
- Nathan MW and Leider M (1962) Studies on bismuth alloys. I. Liquidus curves of the bismuth-copper, bismuth-silver, and bismuth-gold systems. *Journal of Physical Chemistry* 66, 212–5.
- Nockolds RS (1954) Average chemical composition of some igneous rocks. Geological Society of America Bulletin 65, 1007–32.
- O'Neill JM and Lopez DA (1985) Character and regional extent of the Great Falls Tectonic zone, east-central Idaho and west-central Montana. American Association of Petroleum Geologists Bulletin 69, 437–47.
- Oakes CS, Bodnar RJ and Simonson JM (1990) The system NaCl-CaCl₂-H₂O:
 I. The ice liquidus at 1 atm pressure. *Geochimica et. Cosmochim. Acta* 54, 603–10.
- Okamoto H and Massalski TB (1983) The Au-Bi (gold-bismuth) system. Bulletin of Alloy Phase Diagrams 4, 401–7.
- Olinger DA, Andersen AK, Griffis NP, Mercer CM and Smith AJ (2024) Geochemical analyses of rock samples collected from the Judith Mountains and Crazy Mountains alkalic complexes, Montana. U.S. Geological Survey Data Release, https://doi.org/10.5066/P9V4F6VN.
- Oyer N, Childs J and Mahoney JB (2014) Regional setting and deposit geology of the Golden Sunlight Mine. *Geological Society of America Field Trip Guide* 37, 115–44.
- Pals DW and Spry PG (2003) Telluride mineralogy of the low-sulfidation epithermal Emperor gold deposit, Vatoukola, Fiji. *Mineralogy and Petrology* 79, 285–307.
- Pals DW, Spry PG and Chryssoulis S (2003) Invisible gold and tellurium in arsenic-rich pyrite from the Emperor gold deposit, Fiji: implications for gold distribution and deposition. *Economic Geology* 98, 493–514.
- Paterson CJ, Groff NU and Longstaffe FJ (1989) A view through an epithermal-mesothermal precious metal system in the northern Black Hills, South Dakota: a magmatic origin for the ore-forming fluids. *Economic Geology Monograph* 6, 564–70.
- Peterman ZE (1980) Archean gneisses in the Little Ricky Mountains, Montana.
 U.S. Geological Survey Professional Paper 1199-A, 1-6.
- Pirsson LV (1905) Petrographic province of central Montana. American Journal of Science 20, 35–49.
- Porter EW and Ripley EM (1985) Petrologic and stable isotope study of the gold-bearing breccia pipe at the Golden Sunlight deposit, Montana. *Economic Geology* **80**, 1689–706.
- Reich M, Kesler SE, Utsunomiya S, Palenik CS, Chryssoulis SL and Ewing RC (2005) Solubility of gold in pyrite. Geochimica et Cosmochimica Acta 69, 2781–86.
- Richards JP (1995) Alkalic-type epithermal gold deposits A review. In Magmas, Fluids, and Ore Deposits (ed JFH Thompson), pp. 367–400, Mineralogical Association of Canada Short Course Series 23.
- Roedder E (1984) Fluid inclusions. Reviews in Mineralogy 12, 644pp.
- Russell CW (1991) Gold mineralization in the Little Rocky Mountains, Phillipis County, Montana. In *Guidebook to the Central Montana Alkalic Province*; Geology, Ore Deposits and Origin (eds. DW Baker and RB Berg), pp. 1–18. Butte, MT: Montana Bureau of Mines and Geology Special Publication 100.
- Ryzak D (1990) Gold deposits of active mining areas, Little Rocky Mountains, Montana. In Proceedings of the Fourth Western Regional Conference on Precious Metals and the Environment, September 19-22, 1990, Lead, South Dakota, (pp. 61–75) Society for Mining, Metallurgy and Exploration.
- Scherbarth NL and Spry PG (2006), Mineralogical, petrological, stable isotope, and fluid inclusion characteristics of the Tuvatu gold-silver telluride deposit, Fiji: Comparisons with the Emperor deposit. *Economic Geology*, **101**, 135–58.
- Schmidt CJ, O'Neill JM and Brandon WC (1988) Influence of Rocky Mountain foreland uplifts on the development of the frontal fold and thrust belt, southwestern Montana. In *Interaction of the Rocky Mountain Foreland and the Cordilleran Thrust Belt* (eds CJ Schmidt and WJ Perry Jr), pp. 161–201. Geological Society of America Memoir 171.

Sears JW, MacDonald K and Lonn J (2010) Lewis and Clark Line, Montana: Tectonic evolution of a crustal-scale flower structure in the Rocky Mountains. In Through the Generations: Geologic and Anthropogenic Field Excursions in the Rocky Mountains from Modern to Ancient (eds LA Morgan and SL Quane), pp. 1–20. Geological Society of America, Field Guide 18.

- Simmons SF and Christenson BW (1994) Origins of calcite in a boiling geothemal system. American Journal of Science 294, 361–400.
- Simon G, Huang H, Penner-Hahn JE, Kesler SE and Kao L-S (1999) Oxidation state of gold and arsenic in gold-bearing arsenian pyrite. American Mineralogist 84, 1071–9.
- Spry PG, Foster F, Truckle JS and Chadwick TH (1997) The mineralogy of the Golden Sunlight gold-silver telluride deposit, Whitehall, Montana, U.S.A. Mineralogy and Petrology 59, 143–64.
- Spry PG, Paredes MM, Foster F, Truckle J and Chadwick TH (1996) A genetic link between gold-silver telluride and porphyry molybdenum mineralization at the Golden Sunlight deposit, Whitehall, Montana: Fluid inclusion and stable isotope studies. *Economic Geology* 91, 507–26.
- Spry PG and Thieben SE (1996) Two new occurrences of benleonardite, a rare silver-tellurium sulphosalt, and a possible new occurrence of cervelleite. *Mineralogical Magazine* 60, 871–6.
- Spry PG and Thieben SE (2000) The distribution and recovery of gold in the Golden Sunlight gold-silver telluride deposit, Montana, U.S.A. *Mineralogical Magazine* 64, 31–42.
- Spry PG and Thieben SE (1999) The geological, mineralogical, and geochemical characteristics of the Golden Sunlight gold-silver telluride deposit, Montana, U.S.A. In *Mineral deposits: Processes to Processing* (eds CJ Stanley et al.), pp. 939–42: Rotterdam, A.A. Balkema.
- Stacey JS and Kramers JD (1975) Approximation of terrestrial lead isotope evolution by a two-stage model. Earth and Planetary Science Letters 26, 207–21.
- Thieben SE and Spry PG (1995) The geology and geochemistry of Cretaceous-Tertiary alkaline rock-related gold-silver telluride deposits of Montana, USA. In *Mineral Deposits: From their Origin to their Environmental Impacts* (eds J Pašava, B Kříbek and K Žák), pp. 199–202. Rotterdam, A.A. Balkema.
- Thompson TB, Trippel AD and Dwelley PC (1985) Mineralized veins and breccias of the Cripple Creek district, Colorado. *Economic Geology* 80, 1669–88.
- Tilling RI, Klepper MR and Obradovich JD (1968) K-Ar ages and time span of emplacement of the Boulder batholith, Montana. American Journal of Science 266, 671–89.
- Vuke SM, Porter KW, Lonn JD, Lopez DA (2009) Geologic map of Montana field notebook. Montana Bureau of Mines and Geology Geologic Map 62–E, 59.
- Wallace SR (1953) The petrology of the Judith Mountains, Fergus County, Montana. U.S. Geological Survey Open-File Report, 53–265, 189.
- Wallace SR (1956) Petrogenetic significance of some feldspars from the Judith Mountains, Montana. *Journal of Geology* 64, 369–84.

- Warr LN (2021) IMA-CNMNC approved mineral symbols. Mineralogical Magazine 52, 291–320.
- Weed WH and Pirsson LV (1898) Geology and mineral deposits of the Judith Mountains of Montana. U.S. Geological Survey Annual Report 18, 437–616
- Williams-Jones AE and Heinrich CA (2008) Vapor transport of metals and the formation of magmatic-hydrothermal ore deposits. *Economic Geology* 100, 1287–312.
- Wilson MR and Kyser TK (1988) Geochemistry of porphyry-hosted Au-Ag deposits in the Little Rocky Mountains, Montana. *Economic Geology* 83, 1329–46
- Woodward LA (1995) Metallic mineral deposits of the Judith Mountains, central Montana. Montana Bureau of Mines and Geology Memoir 67, 78.
- Woodward LA and Giles DL (1993) Lode mineralization in the Judith Mountains, Montana. In Energy and Mineral Resources of Central Montana (ed LD Hunter), pp. 187–214. Butte, MT: Montana Geological Society Guidebook.
- Yanagisawa F and Sakai H (1983) Thermal decomposition of barium sulfatevanadium pentoxide-silica glass mixtures for preparation of sulfur dioxide in sulfur isotope ratio measurements. Analytical Chemistry 55, 985–7.
- **Zartman RE and Doe BR** (1981) Plumbotectonics The model. *Tectonophysics* **75**, 135–62.
- Zhai D, Liu J, Ripley EM and Wang J (2015) Geochronological and He–Ar–S isotopic constraints on the origin of the Sandaowanzi gold-telluride deposit, northeastern China. *Lithos* 212-215, 338–52.
- Zhai, D, Williams-Jones AE, Liu J, Tombros SF and Cook NJ (2018) Mineralogical, fluid inclusion, and multiple isotope (H-O-S-Pb) constraints on the genesis of the Sandaowanzi epithermal Au-Ag-Te Deposit, NE China. *Economic Geology* 113, 1359–82.
- Zhang X and Spry PG (1994a) Calculated stability of aqueous tellurium species, calaverite and hessite at elevated temperatures. *Economic Geology* 89, 1152–66.
- Zhang X and Spry PG (1994b) Petrological, mineralogical, fluid inclusion, and stable isotope studies of the Gies gold-silver telluride deposit, Judith Mountains, Montana. *Economic Geology* **89**, 602–27.
- Zhang X and Spry PG (1991) Mineralogical and fluid inclusion characteristics of the epithermal Gies gold-silver telluride deposit, Judith Mountains, Fergus County, Montana: A preliminary study. In *Guidebook to the Central Montana Alkalic Province; Geology, Ore Deposits and Origin*. (eds DW Baker and RB Berg), pp. 63–76, Butte, MT: Montana Bureau of Mines and Geology Special Publication 100.
- Zhao G, Zhai D, Keith M, Voudouris P, Tombros S, Zhang H and Liu J (2025) Sulfur and He-Ar isotopic constraints on the origin of alkalic-type epithermal Au-Ag-Te deposits: Insights from the Golden Sunlight deposit, Montana, USA. Ore Geology Reviews 176, 106435.
- **Zhu Y, An F and Tan J** (2011) Geochemistry of hydrothermal gold deposits: a review. *Geoscience Frontiers* **2**, 367–74.